https://doi.org/10.5194/egusphere-2026-3141
Preprint. Discussion started: 17 June 2026

A synoptic-dynamic interpretation of the Southern Annular Mode

Michael A. Barnes[1,2,3], James S. Risbey[4], Teresa J. Parker[4], Nicholas Earl-Jones[5], Carly Tozer[4], and Didier P. Monselesan[4]

[1]ARC Centre of Excellence for 21st Century Weather, Monash University, VIC, Australia
[2]School of Earth, Atmosphere and Environment, Monash University, VIC, Australia
[3]Department of Geography, Geoinformatics and Meteorology, University of Pretoria, Pretoria, South Africa
[4]Environment, CSIRO, Hobart, TAS, Australia
[5]School of Geography, Planning, and Spatial Sciences, University of Tasmania, Hobart, TAS, Australia

Correspondence: Michael A. Barnes (michael.barnes@monash.edu)

Abstract. In this study, we describe the Southern Annular Mode (SAM) as a function of regional extratropical variability in order to understand the synoptic-dynamic features associated with it. The SAM is often considered to be the leading mode of variability in the extratropics and is used to interpret changes and impacts in the large-scale mid-latitude circulation and surface weather in the Southern Hemisphere. This interpretation of the SAM has however been questioned in recent years, given the SAM's lack of annularity and weak correlation to surface weather and synoptic features. From this regional perspective, we once again highlight the non-annularity of the SAM and show explicitly how these asymmetries can result in the misinterpretation and misattribution of regional surface weather impacts. Through analysing a set of weather features including Rossby wave breaking (RWB) zones, cyclones and jets, we show the SAM can be interpreted as a function of the RWB characteristics across the hemisphere, in line with similar perspectives of the North Atlantic Oscillation. In fact, changes in the storm track and jets occur locally and non-annularly across the hemisphere in response to regional RWB, in contrast to the annular view assumed by the SAM. This interpretation provides opportunity for further understanding of present and future Southern Hemispheric extratropical variability and its associated surface weather impacts.

1 Introduction

The Southern Annular Mode (SAM) or Antarctic Oscillation is considered to be the leading (e.g. Thompson and Wallace, 2000) and longest-lived (Risbey et al., 2021) mode of variability in the Southern Hemisphere extratropics. The SAM was originally defined in a similar spirit to the North Atlantic Oscillation (NAO) using pressure differences between stations along the Antarctic coast and stations in the mid-latitudes at roughly $40°$S (Marshall, 2003). Similar interpretations of the SAM have also been constructed from gridded model fields using differences in the zonally averaged mean sea level pressure (MSLP) or geopotential height between $40°$ and $65°$S (Gong and Wang, 1999). The leading mode of the Empirical Orthogonal Functions (EOFs) of the MSLP or geopotential height fields are now however more commonly used to represent the SAM.

Fluctuations in large-scale, hemispheric circulation features in the Southern Hemisphere mid-latitudes such as the jet stream and storm track are often interpreted through variability in the SAM index (e.g. Brahmananda Rao et al., 2003; Sen Gupta and England, 2006; Pezza et al., 2008). Variability in the SAM index is frequently used to describe how other large-scale modes

https://doi.org/10.5194/egusphere-2026-3141
Preprint. Discussion started: 17 June 2026

of variability, such as the El Niño–Southern Oscillation (ENSO) (e.g. Ding et al., 2012), Antarctic variability such as sea ice (e.g. Purich et al., 2016), and the stratosphere (e.g. Lim et al., 2021) affect the mid-latitude tropospheric circulation. Most notably, the SAM is used both operationally in national meteorological and hydrological services and in climate research to explain past, present and future variances in surface weather impacts, such as rainfall and temperature on a range of different timescales from days to years (e.g. Hendon et al., 2007; Pezza et al., 2008; Lim et al., 2016; Trewin, 2024).

Despite its widespread use in climate science, the physical meaning and interpretability of the SAM has been questioned in recent years (e.g. Gerber and Vallis, 2005; Simpson and Polvani, 2016; Spensberger et al., 2020). The SAM is most frequently interpreted to represent the north-south displacement of the Southern Hemispheric eddy-driven jet and storm track. Simpson and Polvani (2016) questioned the relationship between the SAM and the position and strength of the jet. That study shows that the relationship is only relevant during austral winter, calling for caution when analysing and attributing jet shifts to the SAM and suggesting that the interpretation of the SAM changes with season. Spensberger et al. (2020) meanwhile show that the interpretation of the SAM changes when including and excluding the Antarctic from an EOF analysis, concluding that the winter SAM can be interpreted as the connectivity of the Antarctic to the mid-latitudes. Notably, that study additionally showed that the distributions of instantaneous weather features such as jet streaks, cyclones and Rossby wave breaking (RWB) and local surface weather (such as temperature and rainfall) are only weakly correlated to the phase of the winter SAM index, calling into question the interpretation of SAM as an expression of the displacement of the storm track.

Although often interpreted as a zonally symmetric, annular phenomenon, regional asymmetries in the SAM do exist and can account for as much as 20% of the variability in the total SAM signal (Fogt et al., 2012; Purich et al., 2025), further complicating its interpretation. For example, in the western Pacific, the strong subtropical jet present during austral winter and spring restricts feedbacks between the eddies and the basic state flow and between the tropics and mid-latitudes in that region (Barnes and Hartmann, 2010; Gillett et al., 2022). This has lead to some interpreting the extended austral winter SAM as indicative of a pulsing of the mid-latitude jet, rather than a meridional shift (e.g. Barnes and Hartmann, 2010). Asymmetries are also shown to be introduced by the tropics as stationary Rossby waves in the South Pacific (associated with the Pacific-South American pattern), associated with tropical modes of variability such as ENSO (e.g. Ding et al., 2012; Fogt et al., 2012; Campitelli et al., 2022).

In some respects, the North Atlantic Oscillation (NAO) is a regionalised version of SAM's Northern Hemispheric counterpart, the Northern Annular Mode (NAM), describing variations in the jets and storm tracks over the North Atlantic (Marshall et al., 2001). This is especially true when comparing the original station-based SAM definition to that of the NAO, which was also initially defined using station-based differences at distinct latitudes. Although describing variability at a range of different timescales, the NAO has been linked by several studies to blocking (e.g. Shabbar et al., 2001; Scherrer et al., 2006; Luo et al., 2007), and these phenomena are by their definition related to one another. Given the association with blocking, some have also interpreted the NAO through the lens of differences in synoptic Rossby wave breaking (RWB) in the North Atlantic. Franzke et al. (2004) and Benedict et al. (2004) linked negative and positive NAO polarities with anticyclonic and cyclonic RWB, respectively. Woollings et al. (2008) however interprets the NAO differently and associates negative and positive NAO polarities with a blocked and unblocked state, respectively. Notably, despite preceding studies suggesting pre-conditioning mechanisms

https://doi.org/10.5194/egusphere-2026-3141
Preprint. Discussion started: 17 June 2026

between blocking and the NAO, Woollings et al. (2008) argues that Rossby wave breaking and the NAO are simply different interpretations of the same phenomenon.

Several attempts have been made to link and correlate the presence of synoptic-scale RWB to the SAM. Berrisford et al. (2007) noted the structural similarities of RWB and the SAM, noting the dipole structure of both of these phenomena. They suggest that "wave breaking and blocking are a local manifestation" of the SAM and that the occurrence of "wave breaking would control a large part of the variability" in the SAM. Despite this assertion, correlation of RWB occurrence to the SAM is relatively generally weak (Spensberger et al., 2020). Several regions of increased correlations of enhanced RWB to the SAM do however exist, most notably in the Pacific and along the Antarctic coastline (Wang and Magnusdottir, 2011; Berrisford et al., 2007). The regions of stronger correlations of RWB to the SAM in well-known surf zones (zones of frequent RWB) of the Southern Hemisphere suggest that RWB is a plausible mechanism for the existence of the SAM, similar to that described for the NAO. We hypothesise that the larger domain of the Southern Hemisphere compared to that of the NAO masks the true association between RWB and the SAM as suggested by Berrisford et al. (2007).

Given the success of describing the regionally-defined NAO through the lens of synoptic features, in particular RWB zones, and the questions still surrounding the physical interpretation of the SAM, this study aims to view the SAM from a regional, synoptic meteorological perspective. Using this regionalised SAM framework, we pose the following two questions: 1) Given the asymmetry of the SAM, how well does the SAM represent the synoptic meteorology and the associated weather across the hemisphere? 2) Can a regional, synoptic-dynamic perspective provide a useful and consistent interpretation of the SAM?

In order to answer these questions, we define a set of regional SAM indices and demonstrate that they relate to and describe the full signal of the SAM (Section 3). The imprints of regional versus hemispheric perspectives of the SAM are compared, and we demonstrate whether a hemispheric SAM index reasonably represents impacts at the local scale (Section 4). Through the lens of identified weather features (jets, cyclones and RWB) and regional SAM indices, we provide a synoptic-dynamic interpretation of the SAM (Sections 5 and 6). Finally, case studies are used to understand both the annularity and synoptic interpretation of the SAM in the real world (Section 7).

2 Data and methods

European Centre for Medium-range Weather Forecasting reanalysis version 5 (ERA5) data is used throughout this study (Hersbach et al., 2020). Anomalies are calculated from a daily mean climatology for the period 1980 - 2023. Given the large ocean domain in the Southern Hemisphere, rainfall observations are extremely sparse, making satellite rainfall estimates error-prone, particularly in the mid-latitudes (e.g. Reid et al., 2024). Given that precipitation is produced by the model that is used in this study and despite its potential limitations, daily accumulated rainfall from ERA5 output is used to represent rainfall variability in this study.

https://doi.org/10.5194/egusphere-2026-3141
Preprint. Discussion started: 17 June 2026

2.1 SAM index

The SAM index is calculated using the method of Gong and Wang (1999) across the entire Southern Hemispheric domain by

$$hSAM = \overline{MSLP}^*_{40^\circ S} - \overline{MSLP}^*_{65^\circ S} \quad (1)$$

where $\overline{MSLP}^*$ is the normalised daily zonal mean MSLP. The SAM index of Gong and Wang (1999) is preferred over the more typical EOF-based methods as this version more closely resembles the original, station-based version of the SAM which presumably was grounded in a "physically-based intuition" (Spensberger et al., 2020). The SAM index (Equation 1) which calculates the SAM across the entire hemisphere will be referred to as the hemispheric SAM (hSAM) index. We additionally assess regional variations in the SAM index. To do this, the SAM index of Gong and Wang (1999) is recalculated in sectors of 10° with

$$rSAM_i = \overline{MSLP}^*_{i,40^\circ S} - \overline{MSLP}^*_{i,65^\circ S},\ i \in \{-180, -170, ..., 160, 170\} \quad (2)$$

where i represents sectors of 10° longitude. These sectoral SAM values are referred to as the set of regional SAM (rSAM) indices. Equation 2 generates 36 rSAM indices are generated together with the hSAM index from Equation 1. The rSAM indices are named based on the starting longitude for which they are calculated. For example rSAM in the 150°E longitude band ($rSAM_{150^\circ E}$) is calculated in the sector ranging from 150° to 159.75°E. Phases of the SAM are distinguished by the magnitude of the value of the index, with positive phases where where the index exceeds 1 and negative phases where the index is less than -1. All other values of the index are considered to be neutral phases of the SAM. A schematic description of both the hSAM and rSAM is shown in Figure 1.

https://doi.org/10.5194/egusphere-2026-3141
Preprint. Discussion started: 17 June 2026

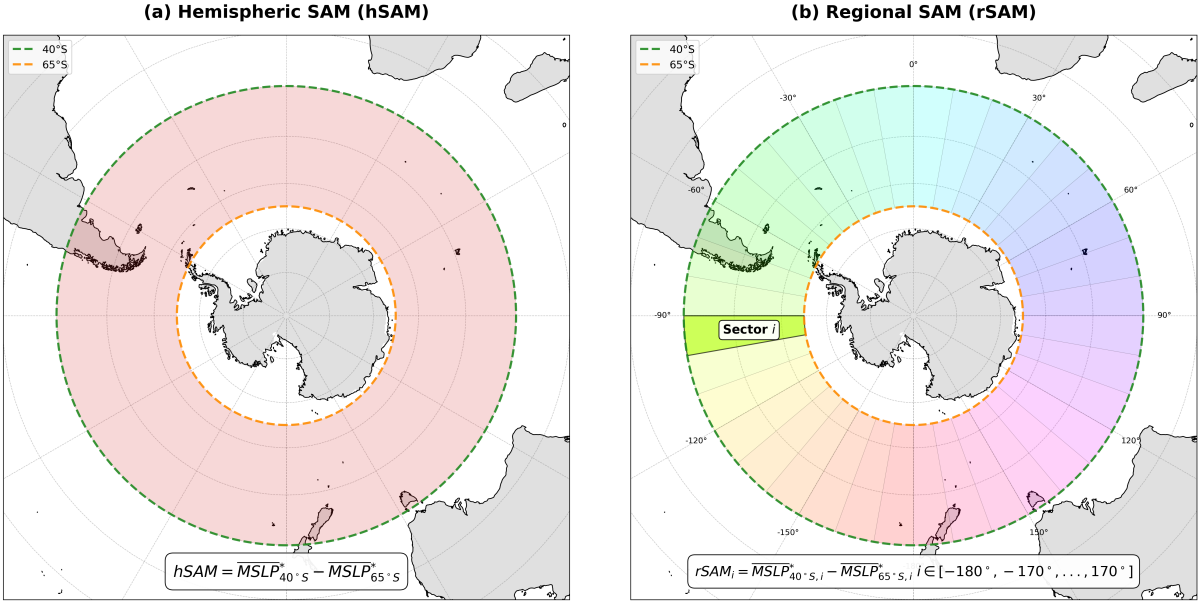

Figure 1. Depiction of the regions and methods defining the hSAM (a) and rSAM (b). Coloured shading simply denote the longitude sectors used. $\overline{MSLP}^*$ denotes the normalised zonal mean MSLP.

2.2 Generalised least squares linear combination

We consider whether a linear combination of all the rSAM indices is a good predicator of the overall hSAM value. To do this, we use a generalised least squares (GLS) solution to account for covariance of each of the rSAMs in the final predicted solution. A simple ordinary least squares (OLS) linear combination was also tested and the results were qualitatively similar, although far noisier.

We first estimate the lag-1 autocorrelation coefficient, ρ, from the residuals of an initial OLS fit. Each transformed predictor is computed as $X_t^* = X_t - \rho X_{t-1}$. This subtracts the autoregressive component associated with the previous timestep from the time series. OLS is then applied to the transformed variables, and the procedure is run iteratively by re-estimating ρ from the updated residuals until the coefficient estimates stabilize.

2.3 Rossby wave breaking

Rossby wave breaking (RWB) is defined here as the irreversible deformation of potential vorticity (PV) contours (e.g. Mcintyre and Palmer, 1983). In this study, we make use of potential temperature on the -2 PV unit (PVU, $1 = 1 \times 10^{-6}\,\mathrm{m^2\,s^{-1}\,K\,kg^{-1}}$) surface, an estimate of the dynamical tropopause. RWB is detected by identifying regions where potential temperature contours on the dynamical tropopause (and therefore where potential vorticity contours on an isentrope) overturn (e.g. Pelly and Hoskins, 2003; Bowley et al., 2019). This is done using a modified version of the algorithm of Kaderli (2024) as used by Barnes et al. (2025). The orientation (anticyclonic or cyclonic) of each RWB zone is calculated by comparing the easternmost

https://doi.org/10.5194/egusphere-2026-3141
Preprint. Discussion started: 17 June 2026

and westernmost latitudes of the overturned contour as in several other studies (e.g. Barnes and Hartmann, 2012; Ndarana and Waugh, 2011; Barnes et al., 2025). The characteristics of each RWB zone are documented, including a rectangular region containing the overturned contour, defining the RWB zone, the centroid of the RWB zone, the orientation (cyclonic or anticyclonic) and its isentropic level.

2.4 Jet and cyclone features

An existing database of jet streaks and cyclones objectively identified from hourly ERA5 reanalyses is used (Sprenger et al., 2017). Cyclones are defined as per Wernli and Schwierz (2006). The algorithm involves identifying regions with a closed contour surrounding a MSLP minimum. Jet streams are defined as per Koch et al. (2006) by identifying regions of mean layer winds speeds between 100 and 500 hPa that exceed 30 $\mathrm{m.s^{-1}}$. More details on the algorithm and other features in the database can be found in Sprenger et al. (2017).

Both the jet and cyclone objects are provided as binary grids at an hourly timestep. Daily jet and cyclone objects are used throughout the analysis and compared to the daily-scale data used in the majority of the analysis. A set of daily weather features is defined by identifying grid cells in which a given feature is present at a grid cell at any hour of each day.

3 Hemispheric versus regional perspectives of the SAM

Figure 2 shows the correlation of various atmospheric variables at each point to the hSAM value for both summer (Figure 2a) and winter (Figure 2b). The patterns expressed are typical of known SAM teleconnections (e.g. Thompson and Wallace, 2000). A poleward shift of the upper-level (300 hPa) zonal mean flow occurs within the mid-latitudes with an increasing hSAM value in both seasons. A strengthening of the subtropical upper-level zonal flow occurs across the majority of all three continents in summer, but is restricted to the African and Southern American continents in winter. A strengthened polar low, marked by a decreasing correlation to 500 hPa geopotential heights with increasing hSAM value, is visible in both seasons. Low-level zonal flow (850 hPa) largely follows that of the upper-level flow with a poleward shift in the mid-latitude westerly flow. Anomalous easterlies are present throughout the subtropics in both seasons, as is often discussed in other studies (e.g. Hendon et al., 2007). Notably however, correlations to the hSAM value are generally small with maximum magnitude of correlation coefficients of between 0.34 - 0.41 in summer and between 0.29 - 0.36 in winter for all three variables shown. The known and documented asymmetries are readily seen in all fields, which appear as an approximately zonal wave-3 pattern as previously identified (e.g. Fogt et al., 2012; Campitelli et al., 2022).

Figures 2c and d show the same correlations for $rSAM_{150^\circ E}$ (rSAM in the 150°E longitude band). Similar to Spensberger et al. (2020), the circulation associated with the regional SAM shows little annularity and its teleconnection is limited to the Australian east coast and the Tasman Sea. Correlation coefficients are much higher than the hSAM value in all fields with maximum magnitudes between 0.55 - 0.7 across all seasons in the vicinity of the 150°E longitude band, while correlations quickly decrease to near zero in other sectors across the hemisphere. Some variables in some sectors are of opposite value. For example, in summer (Figure 2c) the sign of the correlation coefficient of 300 hPa zonal winds to $rSAM_{150^\circ E}$ in the

https://doi.org/10.5194/egusphere-2026-3141
Preprint. Discussion started: 17 June 2026

120-150°W sector within the mid-latitudes is of opposite sign to that in the surrounding region. This suggests that locally, the circulation in the mid-latitudes can be oppositely phased to the hSAM on any given day. Similar local circulation patterns are also observed in other regions across the Southern Hemisphere (see Figures A1-A3).

https://doi.org/10.5194/egusphere-2026-3141
Preprint. Discussion started: 17 June 2026

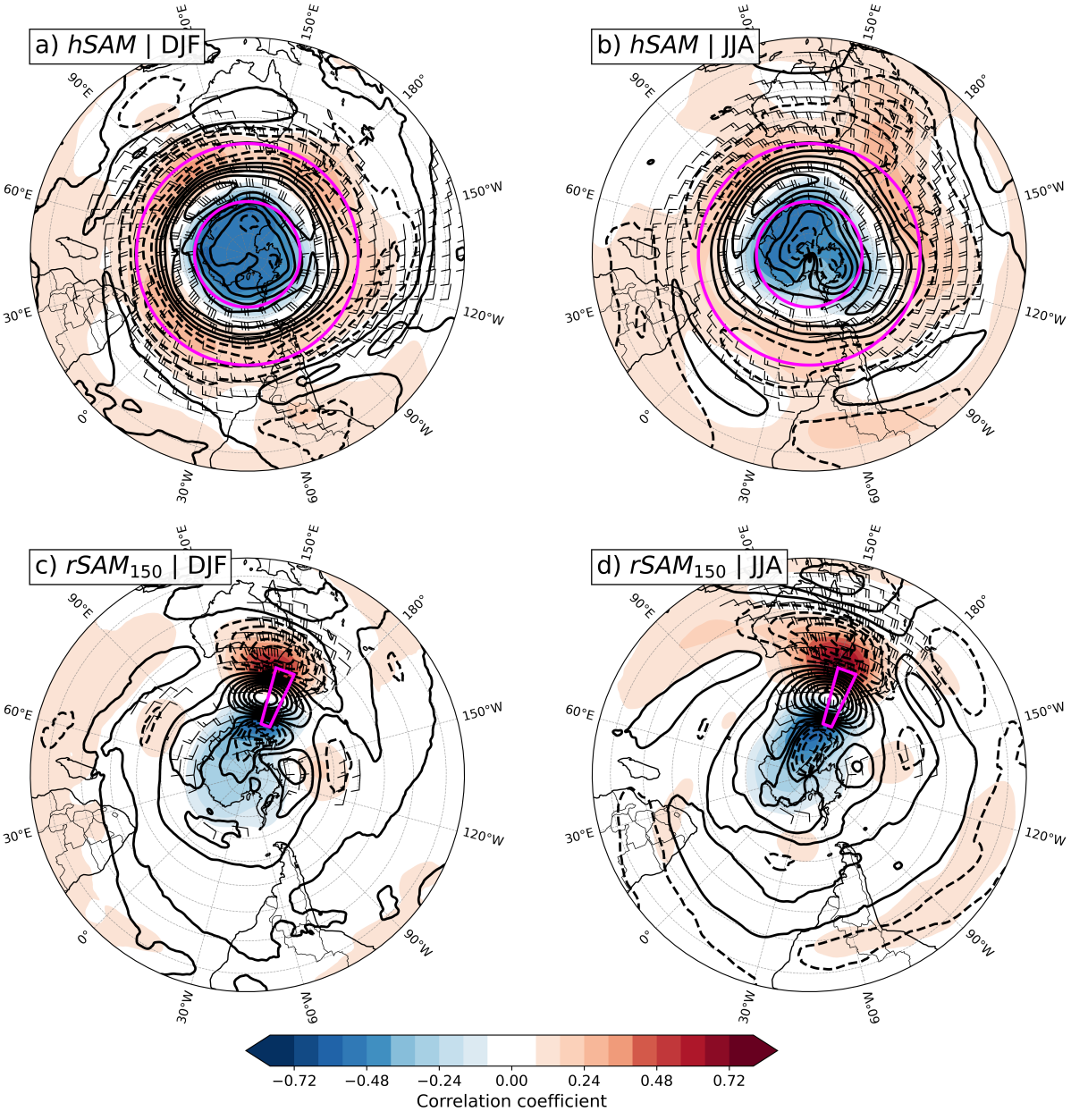

Figure 2. Correlation coefficients of 500 hPa geopotential heights (shading), 300 hPa zonal wind (contours) and 850 hPa zonal wind (barbs) to hSAM (a,b) and $rSAM_{150^\circ E}$ (c,d) for summer (a,c) and winter (b,d). Contours are shown between -0.8 and 0.8 at an interval of 0.08. Wind barb direction shows the sign of correlation (easterly = negative, westerly = positive) while barb feathers indicate magnitude at intervals of 0.05. Barbs are only shown for correlations with a magnitude of greater than 0.1. Regions used in the calculation of SAM are marked by magenta lines.

https://doi.org/10.5194/egusphere-2026-3141
Preprint. Discussion started: 17 June 2026

Given the relatively weak correlations of the hSAM to relatively smooth atmospheric variables such as upper-tropospheric zonal wind and geopotential height, it is perhaps unsurprising that teleconnections to more noisy variables such as 2 m maximum temperature and rainfall are even weaker. Rainfall and 2 m maximum temperature differences between positive and negative hSAM days in summer and winter are shown in Figure 3a and b respectively. Although generally warmer and drier conditions occur along the equatorward edge of the mid-latitudes with wetter and cooler conditions in both the Antarctic and subtropics in positive hSAM phases, the differences are generally weak and not very hemispherically symmetric. Larger rainfall values are seen in the Maritime Continent and western Pacific in both seasons, likely reflecting the interconnectedness of the tropics and mid-latitudes as previously discussed (e.g. Ding et al., 2012). Large temperature differences between winter positive and negative phases of hSAM in the Antarctic presumably reflect the wintertime connection of the SAM to the Antarctic as argued by Spensberger et al. (2020). The cooler temperatures over the Antarctic between positive and negative phases of SAM are still present in summer, but are much weaker.

Figures 3c and d show the differences in surface weather experienced between positive and negative $rSAM_{150°E}$ phases. Similarly to the circulation teleconnections in Figure 2, the differences in weather experienced between rSAM phases are highly localised with much larger magnitudes compared to those associated with the hSAM. Some impacts, particularly around the relevant sector, are completely opposite to those of the same phase of hSAM. For example, a positive hSAM is associated with cooler temperatures over southern Australia in summer, while large positive maximum temperature anomalies occur in positive phases of rSAM in the 150°E sector. Of course, this is to be expected, given that rSAM represents synoptic-scale weather. In particular, a positive rSAM phase in the 150°E sector is indicative of local ridging over the east coast of Australia. These prefrontal conditions are generally associated with heat in the south of the continent (e.g. Reeder et al., 2015). Similarly, in the Tasman Sea to the east of the Australian continent, rainfall is on average suppressed with the ridge associated with positive $rSAM_{150°E}$ while rainfall is on average enhanced with the zonal mean ridging associated with a positive hSAM. This simple example demonstrates that the local circulation, and therefore local weather, is not annular and is therefore not necessarily captured by an index that is intended to be hemispherically symmetric. Similar patterns are also observed in other regions across the Southern Hemisphere (see Figures A1-A3).

https://doi.org/10.5194/egusphere-2026-3141
Preprint. Discussion started: 17 June 2026

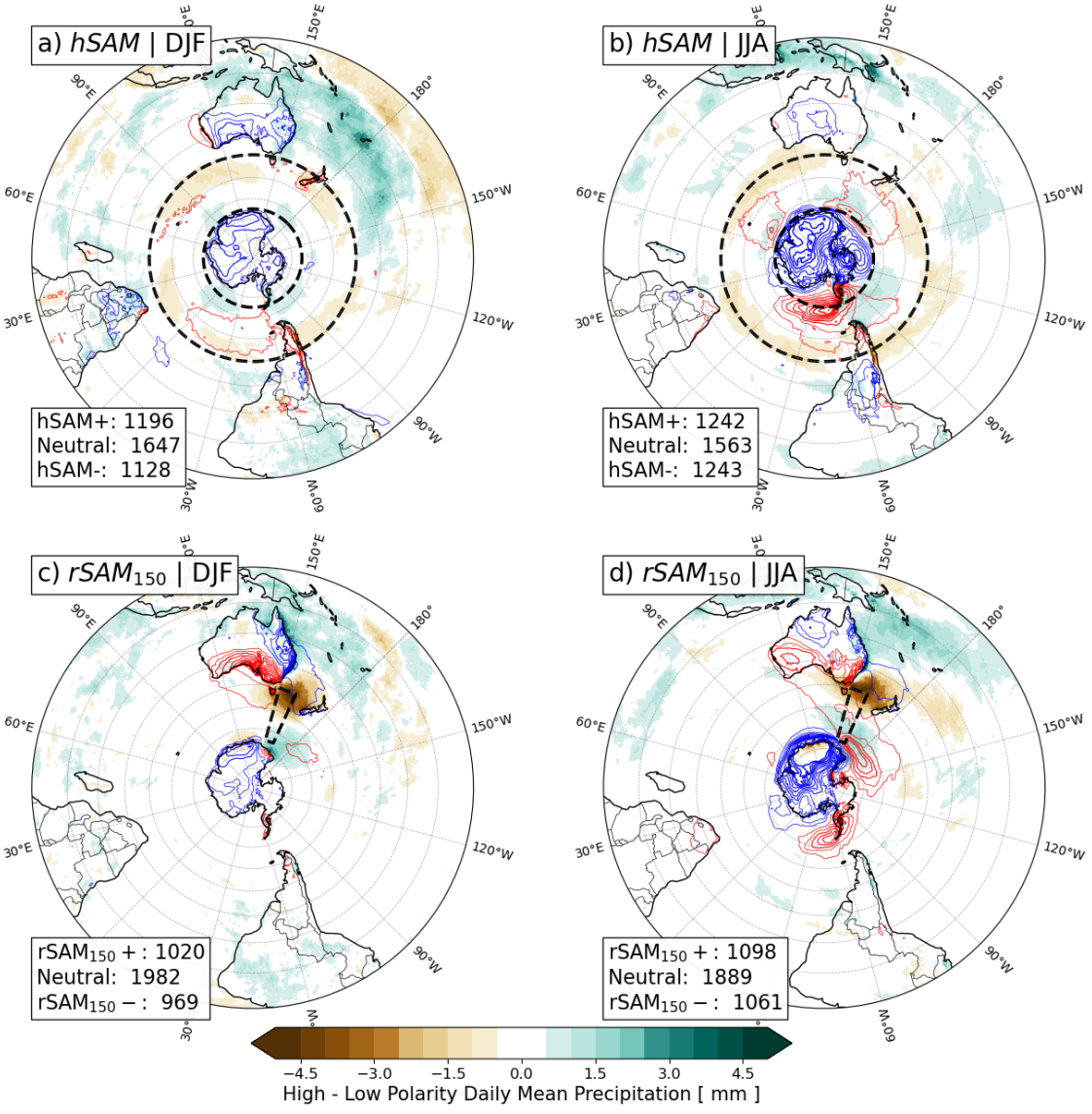

Figure 3. Differences in rainfall (shading) and maximum temperature (positive = red contours, blue = negative, shown at 0.5°C intervals) between high (SAM >1) and low (SAM <-1). Differences using hSAM (a,b) and rSAM in the 150°E longitude band (c,d) are shown for summer (a,c) and winter (b,d). The number of days in each SAM phase (positive, negative and neutral) are shown in the bottom left corner of each panel. Regions used in the calculation of SAM are shown by dashed black lines.

How then do these rSAM values across the hemisphere relate to the hSAM, and do the rSAM values in each sector all vary symmetrically and cohesively?

https://doi.org/10.5194/egusphere-2026-3141
Preprint. Discussion started: 17 June 2026

4 Annularity of the SAM

In order to understand whether the combination of rSAMs describes the full spectrum of the hSAM, we calculate the linear combination of all the rSAM indices to predict the hSAM value as outlined in Section 2.2. Figure 4a shows that the linear combination of all the rSAM indices is a good approximation for the full hSAM index, with an R^2 value of 0.98 and an RMSE of 0.28. The magnitude of the coefficients that describe the linear combination of rSAM sectors are shown in Figure 4b. The different magnitudes of these coefficients show that more weight is given to rSAM values in the Pacific and Tasman Sea, highlighting the large impact that these sectors have on the hSAM. The weakest influence comes from the Indian Ocean, while the influence from the Atlantic sector is more moderate.

Figure 4c shows the correlation coefficients of each rSAM sector to the hSAM. The Indian Ocean sector is the most highly correlated out of all sectors with the overall hSAM index. Taken together with the coefficients from the linear combination (Figure 4b), this suggest that the Indian Ocean sector plays a more passive role: the Indian Ocean varies more closely together with the hSAM, but has a weak impact on the overall hSAM value. Despite the higher correlations in the Indian sector, correlation coefficients are generally low, ranging between 0.39 and 0.52. Somewhat conversely to the Indian Ocean sector, the lowest correlations are found in the Atlantic sector, and in particular in the western Atlantic. This region is one that has a moderate impact on the overall hSAM value (Figure 4b). Correlation coefficients in the Pacific are more moderate with high impact on the overall hSAM value (Figure 4b). The asymmetry in both the impact from each sector and the variation in how correlated with the hSAM each sector is, highlights the asymmetry and lack of annularity of the SAM.

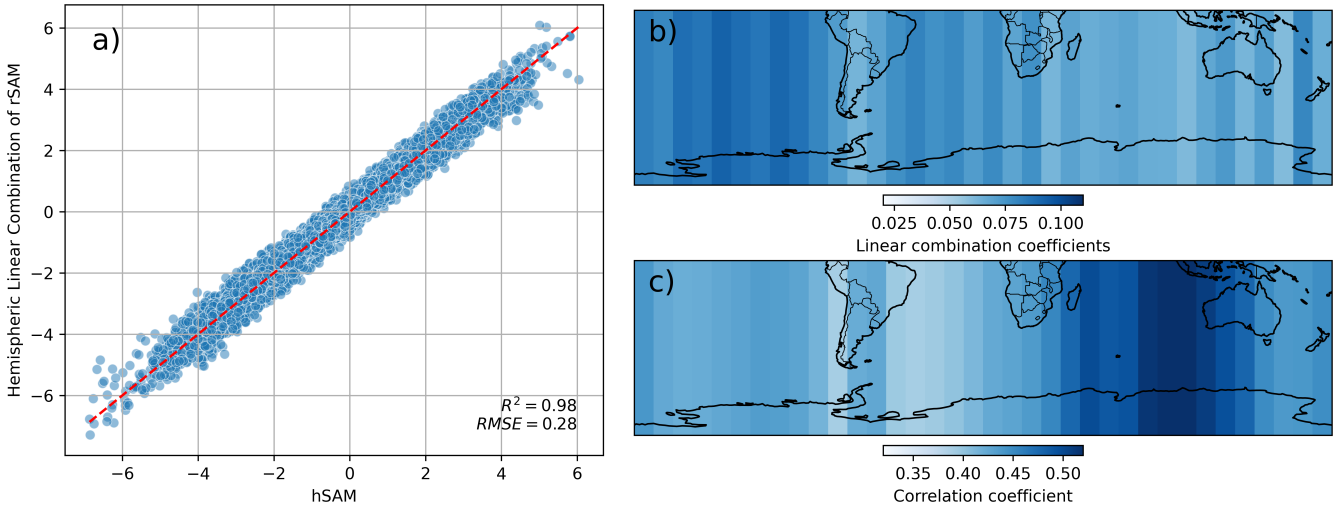

Figure 4. a) Comparison between values of the hSAM and the linear combination of all the rSAMs. Coefficients of the the linear combination of each rSAM sector. c) Correlation coefficients of each rSAM sector to hSAM.

Figure 5 shows the distribution of the number of longitude sectors (out of a total of 36) in which rSAM values are positive, neutral or negative each day, stratified by the hSAM phase. This metric provides a sense of the annularity of the SAM, ex-

https://doi.org/10.5194/egusphere-2026-3141
Preprint. Discussion started: 17 June 2026

pressing the number of sectors that are in a similar phase to the hSAM. If SAM were highly annular, the expectation would be that the majority of rSAM sectors should be in phase with the hSAM (similarly positive or negative) over the majority of the hemisphere. In this scenario, Figure 5 would have large (small) positive (negative) rSAM longitude counts for positive hSAM days and large (small) negative (positive) rSAM counts for negative hSAM days.

Consider positive phases of hSAM, represented on the right-hand side of Figure 5. For moderate positive phases of hSAM (up to values of 2.5), positive rSAM values frequently occur over less than half of the hemisphere. Neutral rSAM values are most frequent during moderate hSAM days while negative rSAM values occur over roughly one quarter of the hemisphere. As the value of hSAM increases, the numbers of neutral and negative rSAM sectors decrease while the number of positive rSAM sectors increases. In the rare, most extreme positive phases of hSAM, the hemisphere does seem to approach annularity. In these extreme cases, positive rSAM sectors span three quarters of the hemisphere and neutral sectors up to one quarter, while negative sectors are rarely present. Similar variability can be observed for negative phases of the SAM as shown on the left-hand side of Figure 5.

The distributions of rSAM sectors in each phase of hSAM suggests that the SAM is rarely truly annular. From this perspective, SAM can only be considered truly annular in its most extreme polarities. Extreme polarities are rare with $|hSAM| > 4.0$ occurring on roughly 2% of days, while neutral SAM ($|hSAM| < 1.0$) are fairly common, occurring on roughly 41% of days. That true annularity only occurs on a small subset of days taken together with Figure 5 suggests that a sector typically has a less than 50% probability of being in the same phase and a 10-25% probability of being in the completely opposite phase as the hSAM. The probability of being in an oppositely-phased rSAM sector is in line with other estimates of SAM asymmetries (e.g. Fogt et al., 2012).

https://doi.org/10.5194/egusphere-2026-3141
Preprint. Discussion started: 17 June 2026

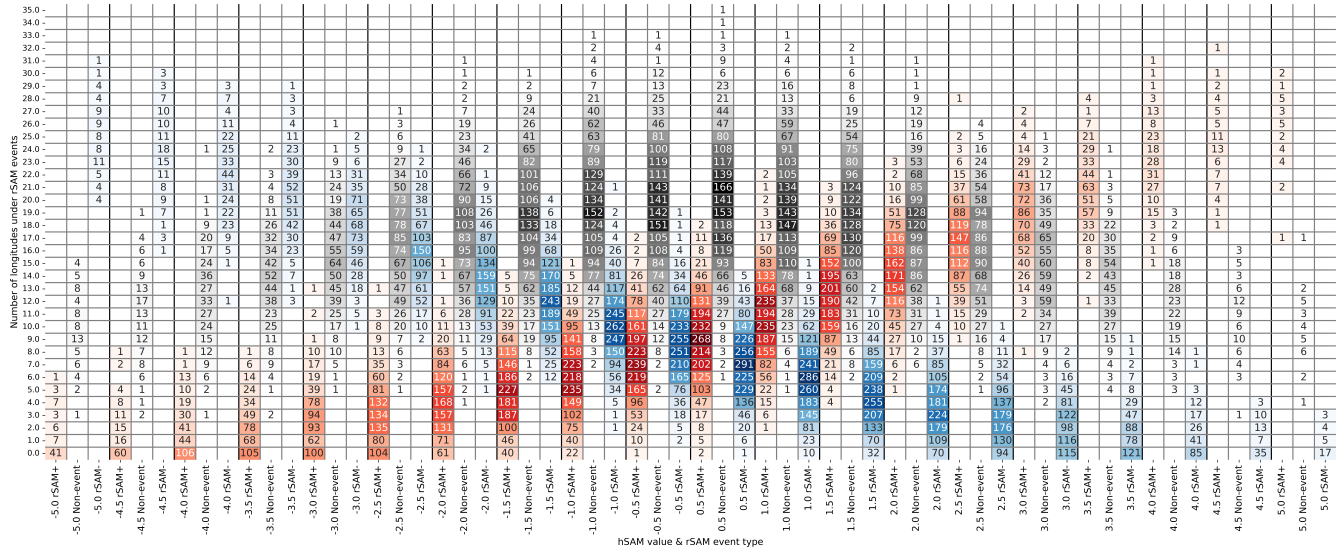

Figure 5. Distribution of the number of longitude bands (rows) of each phase (positive, negative or neutral) of rSAM separated by the overall value of hSAM. Phases of the SAM are grouped into bins of 0.5 and indicated by their inclusive upper-bounds. Columns are labelled by the hSAM phase and value followed by the phase of rSAM (positive, negative or neutral). Colours (blues, reds and greys) reflect the magnitude of the frequency for positive, negative and neutral rSAM values respectively. For example, the bottom leftmost red cell is 41. This indicates that on 41 days with hSAM in the range [-5.0,-4.5), there are 0 longitude sectors (y-axis) that have a positive rSAM (x-axis).

Estimates of the asymmetries of the SAM change depending on the temporal resolution of the calculation. hSAM and rSAM indices are calculated using daily, monthly and seasonal data. For this analysis, the period is extended back to 1960 to increase the number of samples in the monthly and seasonal distributions. Frequencies of the number of longitudes covered by different rSAM phases are calculated as in Figure 5. The median longitude coverage over the 63 year period is shown in Table 1 for daily, monthly and seasonal SAM values.

Table 1a shows the median longitudinal coverage of each phase of rSAM using daily data and highlights the split between in phase, out of phase and neutral rSAM sectors for moderate hSAM values, as shown in Figure 5. When smoothing the time period to monthly (Table 1b) and seasonal (Table 1c) hSAM, the annularity increases with fewer out of phase and more in phase rSAM sectors compared to the hSAM value. The change in annularity with increasing time period is different to that shown by Fogt et al. (2012), who finds that SAM on seasonal timescales loses annularity compared to monthly or annual calculations. This result demonstrates that different methodological approaches provide a different interpretation of the symmetry and processes associated with the SAM, producing a number of different physical interpretations.

5 Synoptic interpretation of coherent rSAM sectors

Given that the hSAM can be expressed as a linear combination of rSAMs, the synoptic meteorology of rSAMs can be used to understand that of the hSAM. Advances in understanding the conceptual picture of the NAO have been gained through

https://doi.org/10.5194/egusphere-2026-3141
Preprint. Discussion started: 17 June 2026

Table 1. Median of the number of positive, negative and neutral rSAM sectors per hSAM range based on daily (a), monthly (b) and seasonal (c) calculated SAM values for the period 1960 - 2023.

a) Daily	-4.0	-3.5	-3.0	-2.5	-2.0	-1.5	-1.0	-0.5	0.5	1.0	1.5	2.0	2.5	3.0	3.5	4.0
rSAM+	1	2	2	3	4	5	6	7	9	11	12	15	17	19	21	23
rSAM-	22	20	18	16	14	12	10	9	7	6	5	3	3	2	1	1
Neutral	13	13	15	17	18	19	19	20	20	19	19	18	17	15	14	12
b) Monthly	-4.0	-3.5	-3.0	-2.5	-2.0	-1.5	-1.0	-0.5	0.5	1.0	1.5	2.0	2.5	3.0	3.5	4.0
rSAM+	0	0	0	0	1	3	4	6	9	11	15	19	23	26	28	29
rSAM-	28	25	22	22	19	14	11	8	7	3	2	1	0	0	0	0
Neutral	8	9	12	13	16	18	20	22	20	20	18	15	12	10	7	5
c) Seasonal	-4.0	-3.5	-3.0	-2.5	-2.0	-1.5	-1.0	-0.5	0.5	1.0	1.5	2.0	2.5	3.0	3.5	4.0
rSAM+	0	0	0	0	0	2	3	6	9	11	16	20	24	28	29	28
rSAM-	30	28	24	23	19	15	12	10	6	4	0	0	0	0	0	0
Neutral	5	7	8	13	16	18	20	21	22	21	19	15	11	8	7	7

understanding the synoptic meteorological view of the NAO, which is essentially a regional version of the NAM. To sectorise the SAM, we isolate coherent structures that describe the SAM out of rSAM sectors and diagnose them from a synoptic meteorological perspective.

Coherent rSAM sectors are defined as a region spanning at least 3 consecutive positive or negative rSAM sectors. Given the findings linking RWB to the SAM (e.g. Berrisford et al., 2007; Wang and Magnusdottir, 2011; Spensberger et al., 2020) and the NAO (e.g. Franzke et al., 2004; Woollings et al., 2008), we determine whether RWB zones occur in proximity to a coherent rSAM sector. A RWB event is considered linked to an rSAM sector if the identified RWB zone intersects with a given rSAM sector.

The percentage of coherent rSAM events associated with cyclonic or anticyclonic RWB, where both orientations occur, or where RWB is absent are shown in Figure 6a and b. Both coherent positive and negative rSAM sectors are linked to RWB structures, with only 17% of positive and 22% of negative coherent rSAM sectors not associated with a RWB zone. Positive coherent rSAM sectors are associated more frequently with an anticyclonic orientation, with 43% of positive coherent rSAM sectors co-located with only an anticyclonic RWB zone, 14% co-located with a cyclonic structure, and 26% co-located with both an anticyclonic and cyclonic RWB zone. Conversely, the dominance of anticyclonic RWB does not exist in negative coherent rSAM sectors, with almost equal detections of anticyclonic (30%) and cyclonic (27%) RWB zones.

It is however the relative position and isentropic level of the different RWB morphologies that is the most striking difference between positive and negative coherent rSAM sectors. Figure 6 shows the density of the centroids of RWB zones associated with coherent rSAM sectors relative to the centre of positive (Figure 6a) and negative (Figure 6b) coherent rSAM sectors, while

https://doi.org/10.5194/egusphere-2026-3141
Preprint. Discussion started: 17 June 2026

Figures 6c and d show the density of the centroids of RWB zones relative to the isentropic levels on which the RWB zones occur. RWB zones are additionally subdivided into anticyclonic (red) and cyclonic (blue) orientations. RWB orientations during positive coherent rSAM sectors occur as a dipole, with majority cyclonic RWB on the poleward edge (65°S) and anticyclonic RWB on the equatorward edge (40°S) of the mid-latitudes. Cyclonic RWB during positive coherent rSAM sectors tend to occur on lower isentropes (290-330 K) while anticyclonic RWB tends to occur on higher isentropes (310-360 K). Conversely, RWB occurring during negative coherent rSAM sectors is more symmetric. Both cyclonic and anticyclonic RWB occur most frequently centred in the middle of the mid-latitudes (52.5°S) and both occur on similar isentropes (300-340 K). A secondary maximum of anticyclonic RWB also occurs equatorward and upstream of the mid-latitudes (centred on 32.5°S).

https://doi.org/10.5194/egusphere-2026-3141
Preprint. Discussion started: 17 June 2026

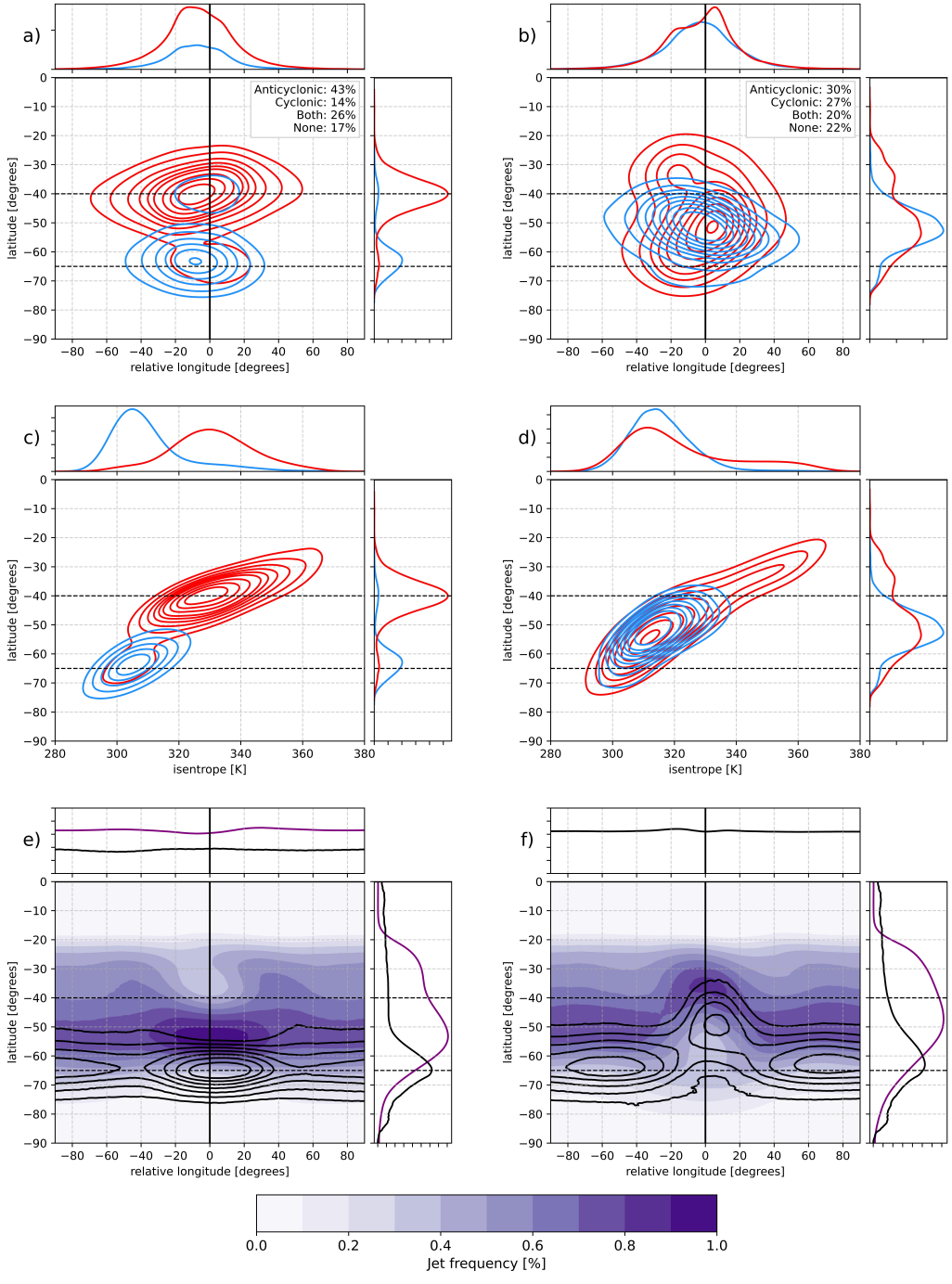

Figure 6. Rossby wave breaking, cyclones and jets identified for positive (left) and negative (right) coherent rSAM sectors. a,b) Density between 0 and 1 at intervals of 0.1 of centroids for anticyclonic (red) and cyclonic (blue) RWB. c,d) Density between 0 and 1 at intervals of 0.1 of isentropes for anticyclonic (red) and cyclonic (blue) RWB. e,f) Cyclone (contours) and jet (shading) frequencies in percent. Contours show values between 0.2 and 1 at intervals of 0.1. Zonal and meridional frequency distributions and densities are shown above the x and y axes of each subplot.

https://doi.org/10.5194/egusphere-2026-3141
Preprint. Discussion started: 17 June 2026

Notably, the frequency of detected RWB zones and the positional and isentropic differences between positive and negative coherent rSAM sectors is relatively consistent across seasons. The dipole structure of RWB frequencies seen in Figure 6 during positive coherent rSAM sectors and the monopole structure within the mid-latitudes during negative coherent rSAM sectors is present across all seasons (not shown). The frequency distribution of the detected types additionally changes little per season as shown in Figure 7. This is particularly true for positive coherent rSAM sectors with each category changing by no more than 6% across seasons. There is a larger frequency shift between cyclonic and anticyclonic types during negative coherent rSAM sectors from the warm to cool season. This frequency difference is reflective of the secondary anticyclonic RWB maximum equatorward of the mid-latitudes in negative coherent rSAM sectors (Figure 6d). This secondary maximum is present during spring, summer and autumn (not shown), but is absent during winter. The absence of this equatorward maximum is consistent with the known dominance of anticyclonic RWB in the summer on the dynamical tropopause of the Southern Hemisphere, particularly on higher isentropes (e.g. Ndarana and Waugh, 2011; Barnes et al., 2025).

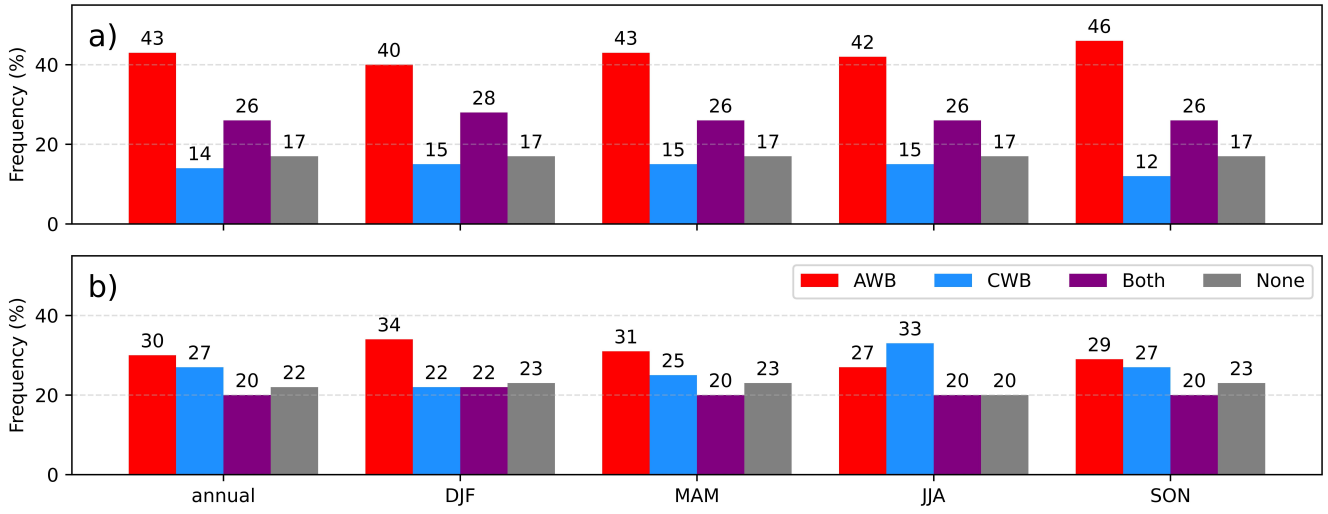

Figure 7. Frequencies of RWB orientation associated with positive (a) and negative (b) coherent rSAM sector per season (summer = DJF, autumn = MAM, winter = JJA and spring = SON). The percentage of all coherent rSAM sectors associated with anticyclonic RWB (AWB, red), cyclonic RWB (CWB, blue), where both types are present (Both, purple) and where none are present (None, grey) are shown.

As the SAM is often associated with changes in the position of the mean state jets and storm tracks, we now analyse the frequency shifts in these features with coherent rSAM sectors. Figures 6e,f show the frequencies of detected cyclones and jet features relative to the centre of coherent rSAM sectors. Positive coherent rSAM sectors show little signature of a mean latitudinal jet shift or cyclone frequency shift. Instead, both jet and cyclone frequencies increase locally relative to the surrounding, climatological frequency. Enhanced jet frequencies are equally observed on the flanks of the positive coherent rSAM sector, extending into the subtropics, while a minimum frequency occurs equatorward of the positive coherent rSAM sector.

https://doi.org/10.5194/egusphere-2026-3141
Preprint. Discussion started: 17 June 2026

Conversely, negative coherent rSAM sectors are indeed associated with a latitudinal shift in the frequency of cyclones from the southern edge of the mid-latitudes into the mid-latitudes. The jet frequency likewise shifts equatorward, with the highest jet frequency located on the northern edge of the mid-latitude zone. Notably, however, this equatorward shift, often associated with negative SAM phases, occurs only locally within the coherent rSAM sector. The climatological jet axis, depicted here as the maximum in jet frequency away from the coherent rSAM sector, changes little between positive and negative phases, shifting from 55°S (in positive phases) to 50°S (in negative phases). This could be a signature of a large-scale jet shift. Given that the remainder of the hemisphere has a higher probability of being in a neutral or similarly phased rSAM (see Figure 5), the small latitudinal shift in the mean state jet frequency could be a reflection of similarly phased coherent rSAM sectors impacting the surrounding mean state.

6 Links between the meteorology of Rossby wave breaking and SAM

Section 5 shows that coherent rSAM events have distinct RWB signatures and are associated with local changes in the jet and cyclone frequencies in the mid-latitudes. Figure 8 shows composites of all RWB zones identified on the 320 K surface and represents the synoptic meteorology surrounding RWB zones. The 320 K surface is chosen as it represents a level on which both cyclonic and anticyclonic RWB frequently occur. Similar qualitative arguments could be made for any chosen isentrope.

Despite the differences in morphology of cyclonic and anticyclonic RWB zones, they have some similar characteristics. RWB by definition represents a reversal in the PV gradient, indicated and detected here by overturning PV contours. The PV gradient reversal in both RWB orientations results in increases in the PV gradient on the poleward and equatorward edges of the RWB zone. It is well understood that jet streams form through strong PV gradients. Unsurprisingly therefore, there is a distinct lack of identified jet objects within the RWB zone where the PV gradient has been reversed. Conversely, jets streams most frequently occur on the poleward and equatorward edges of the RWB zone where the PV gradient has increased. In other words, RWB results in a split jet configuration on average.

Changes in jet frequencies do occur on the poleward edges of the RWB zones between the two different RWB morphologies. Jets are far more frequent on the poleward edge of anticyclonic RWB zones compared to cyclonic RWB zones (Figure 8 c,d). This difference can be explained by the differing dynamics of these morphologies. Anticyclonic RWB is most often poleward directed from the equatorward side of the mean state jet. It is therefore often associated with tropospheric air being advected poleward, tightening the PV gradient in the mid-latitudes. Conversely, cyclonic RWB is often directed equatorward from the poleward side of the mean state jet, with stratospheric air being advected equatorward. The result is a preferential relative latitude at which the strongest jet streaks are formed. This effect is enhanced for higher isentropes where anticyclonic RWB most frequently occurs, and for cyclonic RWB on lower isentropes. It is also noteworthy that Figure 8 shows that on the 320 K surface the latitudinal distance from the centre of the RWB zone to the two split jets is about 15° on average.

Unlike jet streaks, mid-latitude cyclone frequencies change distinctly between cyclonic and anticyclonic RWB morphologies (Figure 8c,d). Cyclones are more frequent in conjunction with cyclonic RWB with their associated deeper PV intrusions of stratospheric PV air than with anticyclonic RWB zones with weaker, shallower PV streamers (e.g. Hoskins et al., 1985; Barnes

https://doi.org/10.5194/egusphere-2026-3141
Preprint. Discussion started: 17 June 2026

et al., 2022). Given these morphologies most typically occur on the poleward edge of the mean state PV gradient and therefore likely within the main storm track, their structure is associated with a local enhancement of cyclones within the RWB zone. A decrease in frequency also occurs in the ridge on the downstream edge of cyclonic RWB zone. Anticyclonic RWB on the other hand is most frequent on the equatorward side of the mean state PV gradient. The ridging associated with it drives the associated jet and cyclones on its upstream edge poleward. A smaller scale enhancement of cyclone frequencies also co-occurs with the PV streamer on the downstream edge of the anticyclonic RWB zone. The net result of anticyclonic RWB in the mean is a split storm track structure.

The structures of coherent rSAM sectors matches that of the general synoptic meteorology of RWB. Any RWB (either cyclonic or anticyclonic) that occurs on the northern or southern boundaries of the mid-latitudes (positive coherent rSAM events) would enhance the frequency of jet streaks within the mid-latitudes. Anticyclonic RWB on the northern boundary of the mid-latitude belt would correspond with enhanced cyclone frequencies on the southern boundary. Cyclonic RWB centred on the southern boundary of the mid-latitudes (65°S) with their associated localised enhancement of cyclone frequencies centred on the southern boundary would produce a pattern similar to that associated with positive coherent rSAM events. Conversely, any RWB that occurs within the central latitudes of the mid-latitudes (around 52.5°S) would produce a split jet structure, enhancing the frequency of jets centred on the northern and southern boundaries and cyclones within the mid-latitude zone.

https://doi.org/10.5194/egusphere-2026-3141
Preprint. Discussion started: 17 June 2026

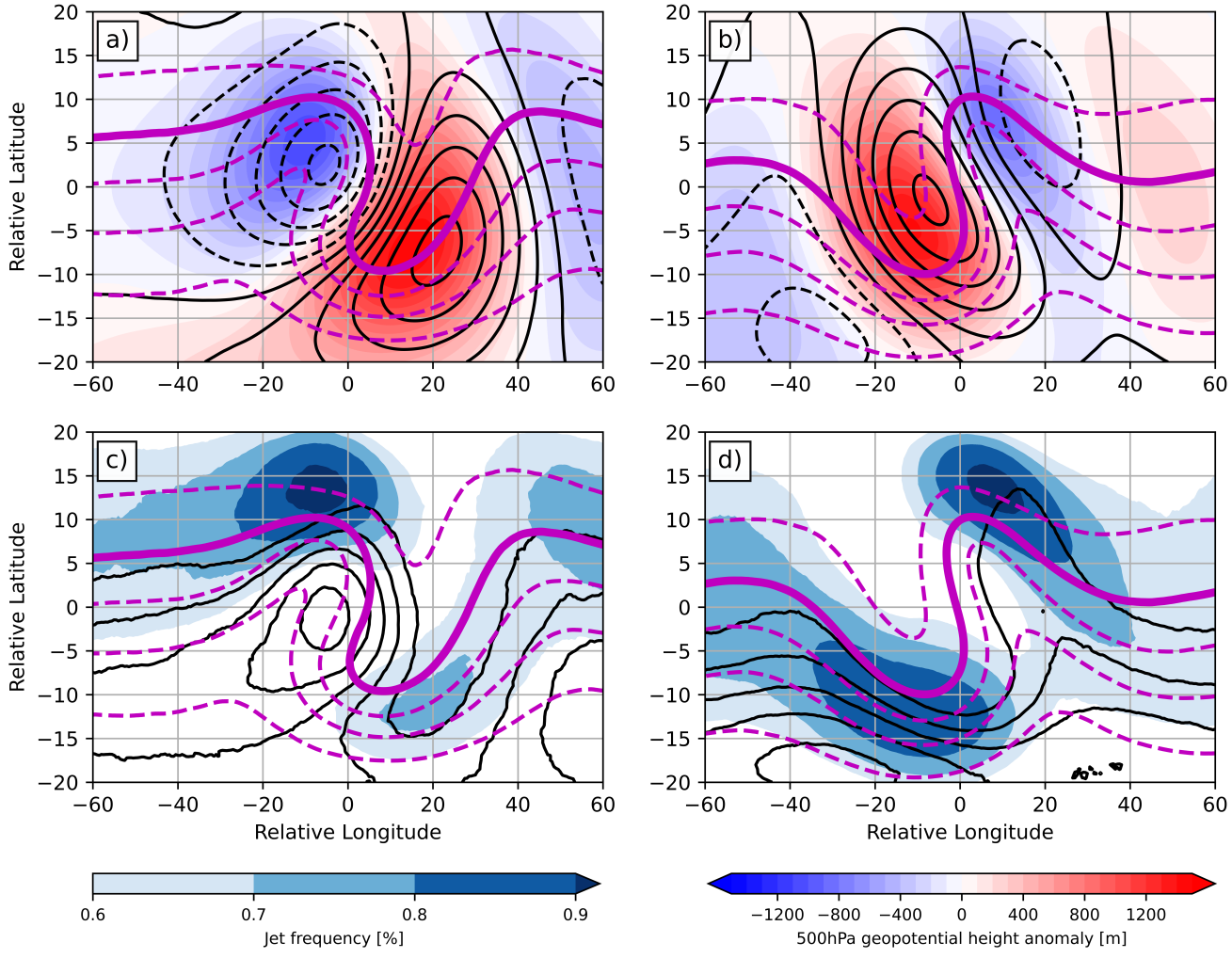

Figure 8. Composites of cyclonic (a,c) and anticyclonic (b,d) RWB relative to the detected centroid identified on the 320 K surface. PV contours in steps of 1 PVU (purple contours) with the -2 PVU contour shown in thick solid lines. Panels a,b): 500 hPa (shading) and MSLP (contours) anomalies. MSLP contours are provided in intervals of 2 hPa with solid contours indicating positive values and dashed contours indicating negative values. Panels c,d): Frequency of jet (shading) and cyclones (contours). Cyclone frequency contours are shown at intervals of 0.1 for frequencies above 0.2.

7 Case studies

Figure 9 shows two examples of the asymmetry of the SAM from the rSAM perspective, demonstrating how they may promote a misdiagnosis of the weather systems and their impacts at a particular location. Both examples demonstrate moderate hSAM

https://doi.org/10.5194/egusphere-2026-3141
Preprint. Discussion started: 17 June 2026

polarities, with hSAM values of -2.0 and 2.1 respectively. Both are examples which centre on days in which rSAM is in opposite phase in the 150° longitude sector to match with the examples in Figure 4.

Figure 9a, showing a day of negative hSAM, has two sectors with strongly positive rSAM values, in the Tasman Sea at 150-160°E and in the African sector at 10-20°E. Over the east coast of Australia, despite a connection to enhanced westerly flow for negative SAM phases, the strong ridge over the Tasman Sea promotes easterly flow over the southeast of the continent. The dynamical tropopause (indicated by the -2 PVU contours in magenta) highlights the RWB that is driving the positive rSAM values over the sector, with a cyclonically overturned structure on the Antarctic side of the jet stream (seen here in green shading and quivers) and an anticyclonically overturned structure on the equatorward side. These cyclonic RWB and anticyclonic RWB structures form on low (315 K) and high (360 K) isentropes as occurs frequently (as shown in Figure 6). This pattern promotes a zonally orientated jet structure in the mid-latitudes. Conversely, in other sectors in which rSAM is negative, the jet stream appears more wavy. The strongest rSAM negative sector neighbours the strong positive rSAM sector east of Australia and occurs across the dateline, in the Pacific Ocean. The wavy jet stream appears as a cyclonically overturned structure on the dynamical tropopause, extending across the entire mid-latitude belt, the centre of which occurs near the central latitudes of the mid-latitude belt (as demonstrated in Figure 6). Although weakly negative rSAM values comprise the majority of the hemisphere, presumably contributing to the overall negative hSAM, several sectors are under the influence of positive SAM-like conditions.

Similarly but opposite to Figure 9a, Figure 9b demonstrates a positive rSAM day. It appears much more symmetric than the negative rSAM example, with weak positive rSAM sectors across the majority of the hemisphere. The exception occurs over the Tasman Sea, where the negative rSAM sector is generated by a cut-off low linked with previous RWB (e.g. Barnes et al., 2021; Ndarana and Waugh, 2010). The jet in this sector resembles a more wavy jet stream, extending far equatorward. A secondary, weaker jet stream is also observed on the poleward edge of the mid-latitudes as occurs generally for coherent negative rSAM events (Figure 6f).

https://doi.org/10.5194/egusphere-2026-3141
Preprint. Discussion started: 17 June 2026

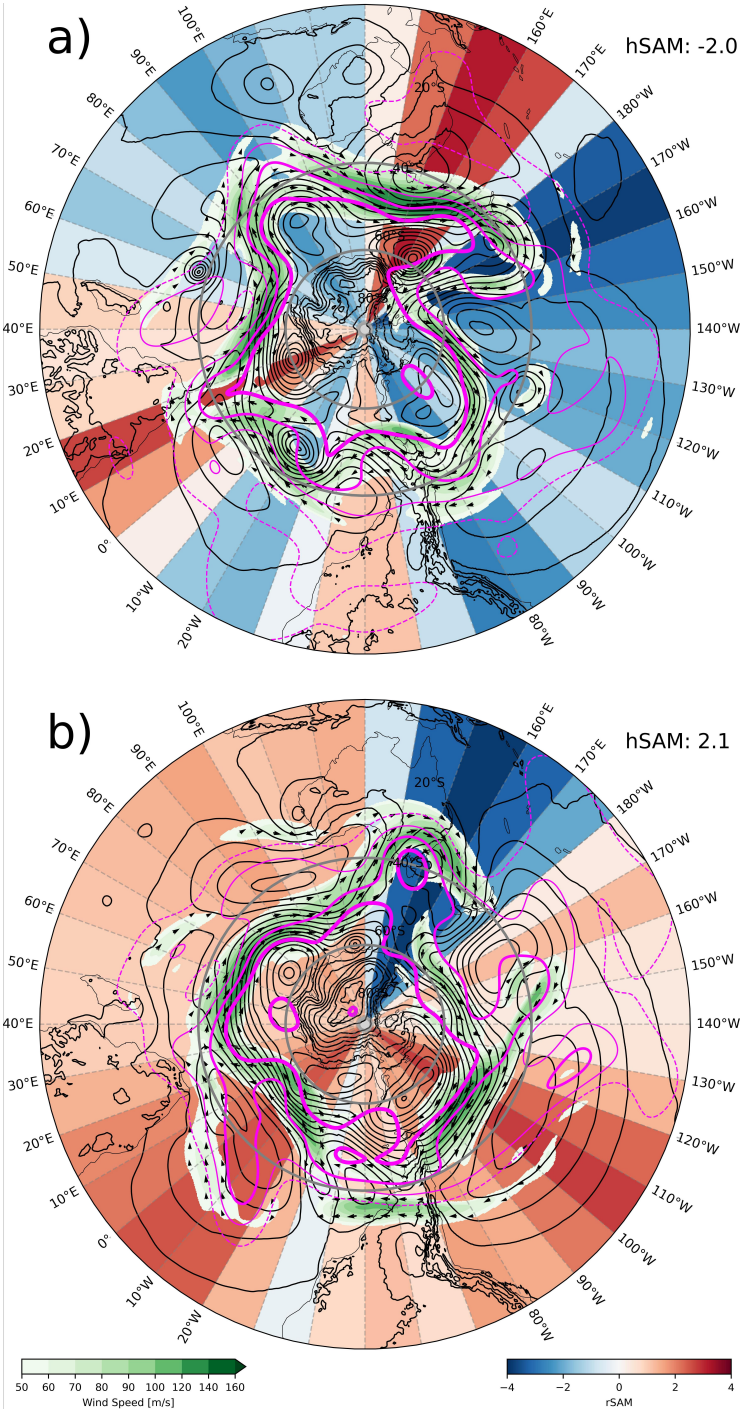

Figure 9. Case studies of negative (a) and positive (b) hSAM events from the rSAM perspective. hSAM values of each case are given at the top right of each panel. Sectoral shading shows the values of each rSAM sector. Jets at 300 hPa defined by wind speeds greater than 30 $\mathrm{m.s^{-1}}$ are depicted by green shading and quivers. -2 PVU contours on the 315, 330, 345 and 360 K isentropic surfaces are shown by thick, moderate, thin and thin dashed magenta contours respectively. MSLP at intervals of 4 hPa are shown in black contours.

https://doi.org/10.5194/egusphere-2026-3141
Preprint. Discussion started: 17 June 2026

8 Discussion and conclusion

In this study, we provide a sectoral, synoptic-dynamic perspective of the SAM by utilising the SAM index of Gong and Wang (1999) (which we name the hemispheric SAM or hSAM), together with a regionalised version of the SAM (which we name the rSAM). The synoptic-dynamic perspective is provided by relating a range of detected weather features including RWB, cyclones and jets to coherent rSAM sectors and linking those sectors to the variability of the hSAM.

The hSAM can be described as a linear combination of the SAM-like characteristics of each region across the hemisphere. These sectoral descriptions of the SAM each have only a weak relationship to the overall SAM value (with correlation coefficients of 0.39-0.52). The highest correlations to the SAM occur in the Indian Ocean sector, perhaps only weakly contributing to the overall SAM value with damped coefficients in the linear combination. The reverse is generally true for much of the Atlantic, while the Pacific has moderate correlations to the hSAM but contributes greatly to the overall hSAM. Given the SAM is well described by the linear combination of rSAMs, the weak correlations are perhaps unsurprising, as the full spectrum over the entire hemisphere is required to recreate the hemispheric value.

Statistics of the rSAM and their relationship with hSAM show that the hSAM is not a truly annular phenomenon, as has been shown by several other studies (e.g. Campitelli et al., 2022). We argue here that these asymmetries are large for the majority of SAM values. For moderate values of SAM, roughly 10-25% of the hemisphere is covered by strong, opposite polarities of the SAM, while between 25-50% of the hemisphere is comprised of weak to neutral values. This suggests that the SAM is potentially a flawed metric for assessing the hemispheric-wide circulation regime on daily timescales. Misgivings about the interpretation of the SAM as an annular mode are aligned with those expressed by Spensberger et al. (2020), who investigated sectoral perspectives of the EOFs that describe the SAM. The increasing annularity with timescale and hSAM magnitude suggests that the SAM is more appropriate for high-magnitude of long-lived events, as suggested by Risbey et al. (2021). How synoptic weather features or events imprint on and impact longer-lived, asymmetric phenomena is still an open question.

Describing coherent rSAM sectors using synoptic weather features reveals that phases of rSAM are associated with different characteristics of RWB morphologies, structures and locations. Positive coherent rSAM sectors are associated with anticyclonic (cyclonic) RWB occurring on higher (lower) isentropes centred on the equatorward (poleward) edges of the mid-latitude belt. As a known signature of RWB (see Figure 8), enhanced frequencies of RWB in the aforementioned locations result in enhanced jet frequencies in the central latitudes and enhanced cyclogenesis on the poleward edge of the mid-latitudes. Conversely, negative coherent rSAM sectors are associated with cyclonic and anticyclonic RWB within the mid-latitude belt, promoting a split jet structure, enhancing jet frequencies outside of the mid-latitudes, in particular on the equatorward edge, and promoting cyclogenesis within the mid-latitudes. Notably, the impacts on the mid-latitudes are local, with close to climatological frequencies outside of coherent rSAM sectors. These results, together with the relatively low number of rSAM sectors in phase with the hSAM, highlight that changes in the storm track (regions of frequent cyclogenesis) and jets occur locally and non-annularly across the hemisphere, in contrast to the annular view assumed by the SAM.

The synoptic-dynamic interpretation of the SAM in this study has some similarities and differences to other studies. Wang and Magnusdottir (2011) show that summer SAM values are impacted by high-latitude cyclonic RWB and low-latitude anti-

https://doi.org/10.5194/egusphere-2026-3141
Preprint. Discussion started: 17 June 2026

cyclonic RWB, which we demonstrate is a good description of the synoptic-dynamics of positive rSAM phases, independent of season. That study notably links changes in the positive trend in the SAM to known surf zones. How exactly these synoptic processes are changing in relation to the trending SAM value in the Southern Hemisphere is still an open question. Spensberger et al. (2020) found through EOF analysis that the SAM correlates little to weather features. Although this may seem at odds with our results, their sectoral results show increased correlations to weather features in similar patterns to those found here. The results of the present study suggests that the zonal mean view of the SAM likely masks correlations to synoptic weather features (for example as shown in Figures 2 and 3). Spensberger et al. (2020) interprets the SAM as the connectivity of the mid-latitudes to the Antarctic. Somewhat counter-intuitively, other studies have shown that the SAM is linked to the variability in the tropics through larger-scale modes of variability (e.g. Ding et al., 2012). The linking of the SAM to RWB zones described in our study unifies these interpretations, as both tropical activity (through both direct and indirect diabatic effects) and polar activity (through the stratospheric polar vortex and cold air outbreaks) impact the mid-latitude waveguide and the Rossby waves that propagate and amplify along it. Future studies that aim to understand how both the tropical and polar regions impact transient waves and RWB locally will likely therefore enhance our understanding of general mid-latitude variability and change.

In the North Atlantic, some interpret NAO polarities to be functions of different orientations of RWB (e.g. Franzke et al., 2004; Benedict et al., 2004). We find this interpretation to be inconsistent for the SAM, as both rSAM polarities are a function of both cyclonic and anticyclonic orientations. Woollings et al. (2008) interprets the NAO from a RWB perspective, with the NAO polarity as either a (high-latitude) blocked state or a basic state. Our results for the SAM show similar characteristics to that interpretation. In their framework, the blocked state presents as a coherent rSAM negative state, with amplified local Rossby wave activity and eventual RWB within the mid-latitudes. RWB centred in the mid-latitudes promotes tropospheric air to be advected poleward, presumably triggering high-latitude blocking diagnostics. We however interpret this state slightly differently, and refer to it as a "highly amplified" or "wavy" state, given the enhancement of waviness in the mid-latitudes. The "basic state" of Woollings et al. (2008) is reminiscent of the coherent positive rSAM state described here, with a strengthened, perhaps more zonal jet within the mid-latitudes (as shown in the Figure 9a). From our results, we interpret this SAM state to be a state of "subtropical and high-latitude" wave activity and breaking. Overall, we interpret different polarities of rSAM to be associated with differences in the latitudinal centring of RWB and therefore the location and amplitude of local wave activity.

Given the hSAM can be described as a linear combination of rSAMs across the hemisphere and given the synoptic characteristics of coherent rSAM sectors, in particular their link to differences in local RWB, we find that the SAM can be interpreted as *the sum of the RWB characteristics across the hemisphere*. Furthering our understanding of mid-latitude variability from this perspective has the ability to advance our understanding of the links between synoptic-scale and climatic scale variability, better understand shifts in warmer climates, and provide more physical links to regional surface weather impacts. The results suggest that caution should be taken when attributing weather and climate impacts to the SAM. Although teleconnections do exist, the links between the SAM and the circulation and impacts are relatively restricted to the Antarctic and sub-Antarctic regions and are generally weaker over the Southern Hemisphere continents. Most critically, as noted by Berrisford et al. (2007), the SAM is a reflection of discrete regions of enhanced RWB, which is not at all annular. Therefore, there are strong imprints

https://doi.org/10.5194/egusphere-2026-3141
Preprint. Discussion started: 17 June 2026

of the local SAM (rSAM) on temperature and rainfall on the proximate continents. These imprints can be of the opposite sign to that expected from hSAM.

When assessing causal links, we propose that consideration be included that attempts to assess the regional differences in local wave activity (such as RWB) when assessing mid-latitude variability. Without such an assessment, dynamically relevant, regional structures can be hidden within the data, introducing interpretation biases and conclusions that do not necessarily have physical consistency. The most optimal assessment of causation is through the analysis of the synoptic-scale weather features themselves (such as cyclones or RWB) that deliver the impacts of interest and which may be prevalent within a sector of interest. However, there are occasions where such an analysis is simply not possible, owing to data availability or volume, or where a simplified view is required. This study demonstrates that a locally-derived SAM index has the potential to be able to act as a proxy for such features as it represents their likely presence or absence. Regional SAM indices have been used over the Australian sector in the past, showing that they better explain rainfall variability (Meneghini et al., 2007) and rainfall trends (Nicholls, 2010) over southern Australia compared to their hemispheric counterparts. Of course, some of the relationship between a local SAM index and the proximate continent is built in by the location of the equatorward component of the index situated on or near the continent. That means that it reflects local pressures over the continent, which builds in some correlation with local rainfall. Future work should further assess how regionally-specific proxies both connect to dynamical structures and aid in furthering our understanding of the weather and climate of the Southern Hemisphere.

Code and data availability. ERA5 reanalysis data is freely available from the Copernicus Climate Data Store (Copernicus Climate Change Service, 2018a, b) and was retrieved from the replicated archive provided by NCI Australia (2020). Jet and cyclone feature detections provided by Sprenger et al. (2017) are available from those authors on request. RWB detections were done using the code of Kaderli (2024), available on GitHub.

https://doi.org/10.5194/egusphere-2026-3141
Preprint. Discussion started: 17 June 2026

Appendix A: Teleconnections of rSAM for selected regional locations

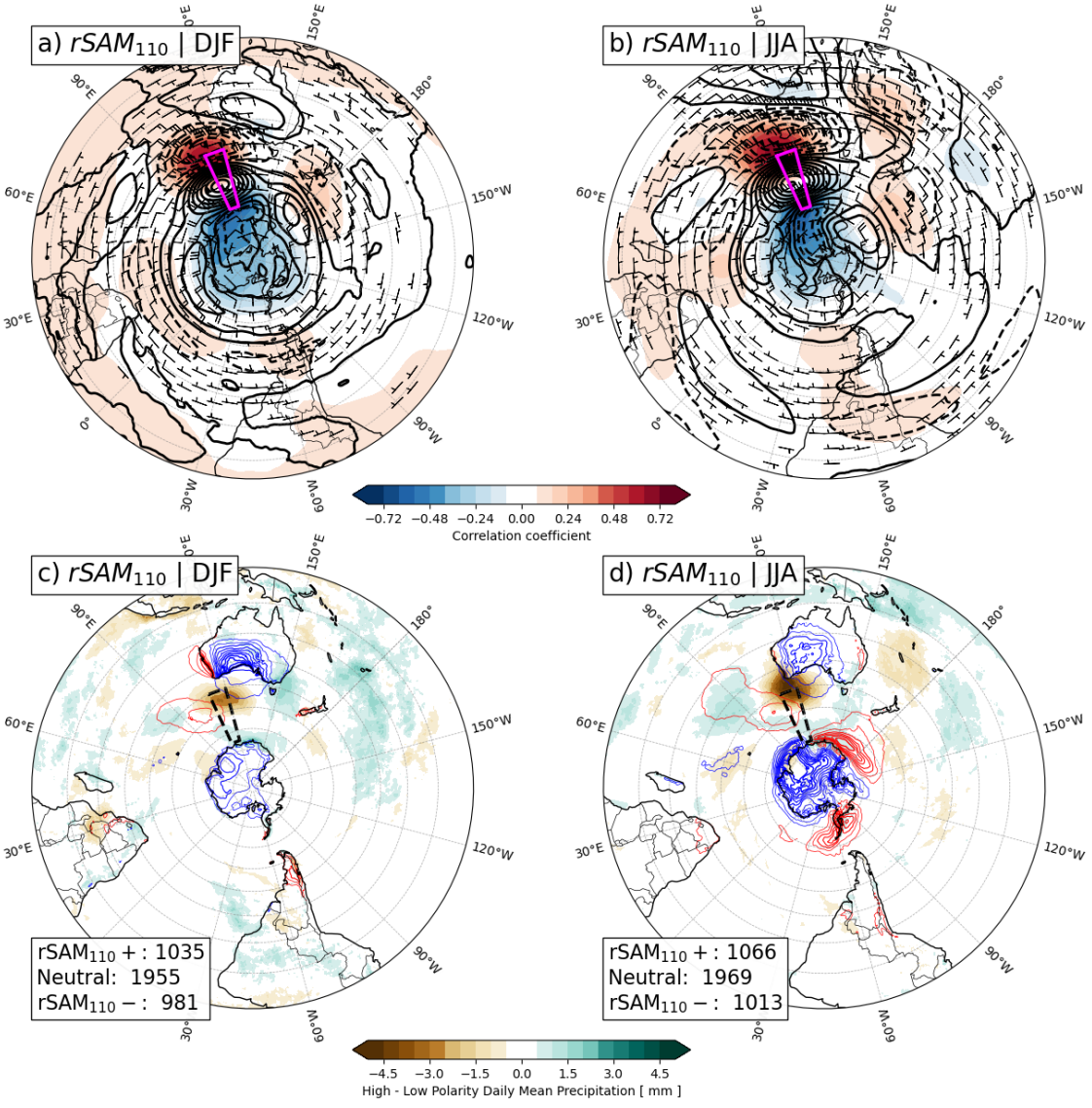

Figure A1. Circulation and weather associated with rSAM in the 110°E longitude band representing the southwestern Australian region. Panels a and b: As in Figure 2c,d. Panels c and d: As in Figure 3c,d.

https://doi.org/10.5194/egusphere-2026-3141
Preprint. Discussion started: 17 June 2026

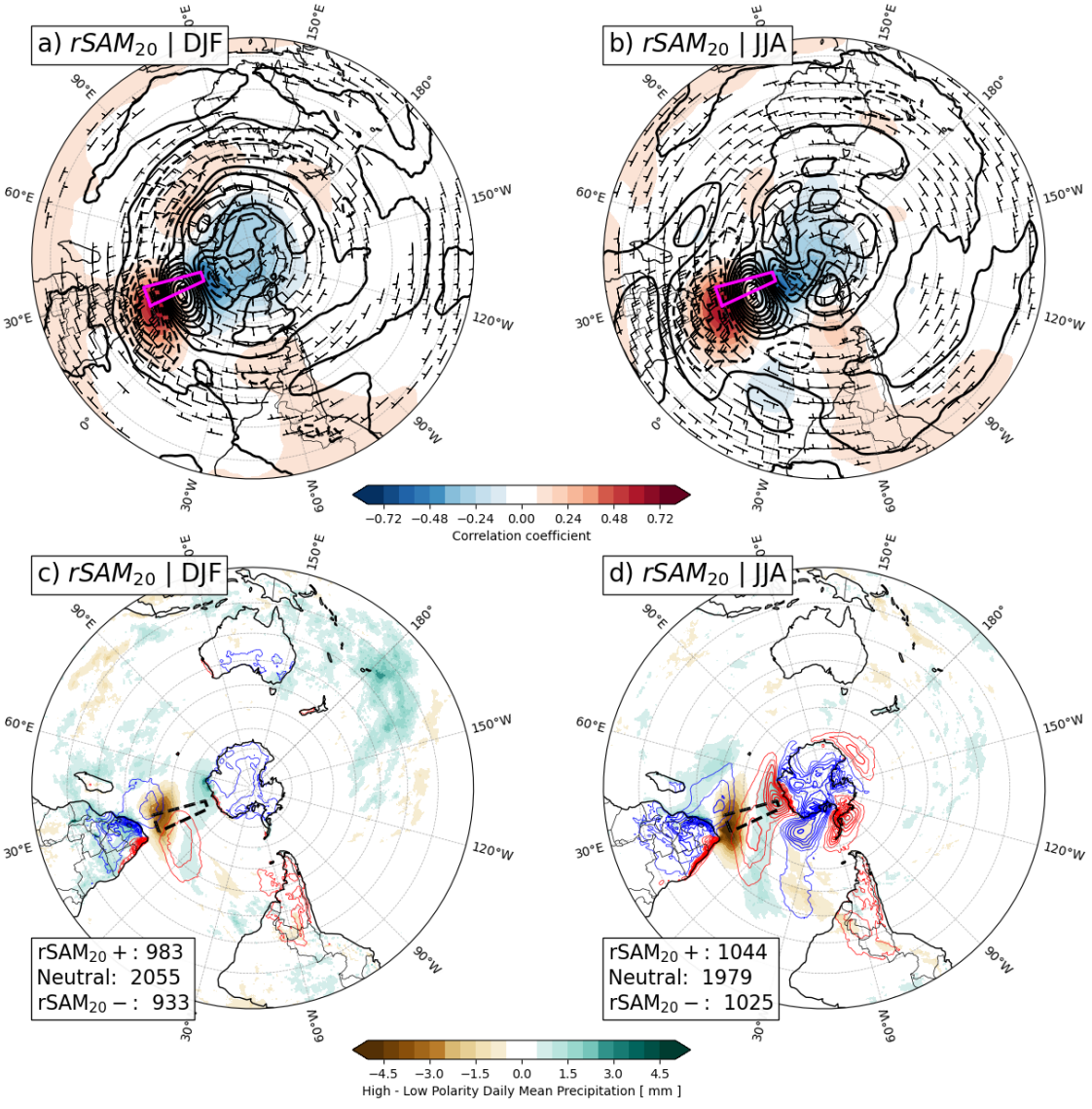

Figure A2. Circulation and weather associated with rSAM in the 20°E longitude band representing the southwestern Australian region. Panels a and b: As in Figure 2c,d. Panels c and d: As in Figure 3c,d.

https://doi.org/10.5194/egusphere-2026-3141
Preprint. Discussion started: 17 June 2026

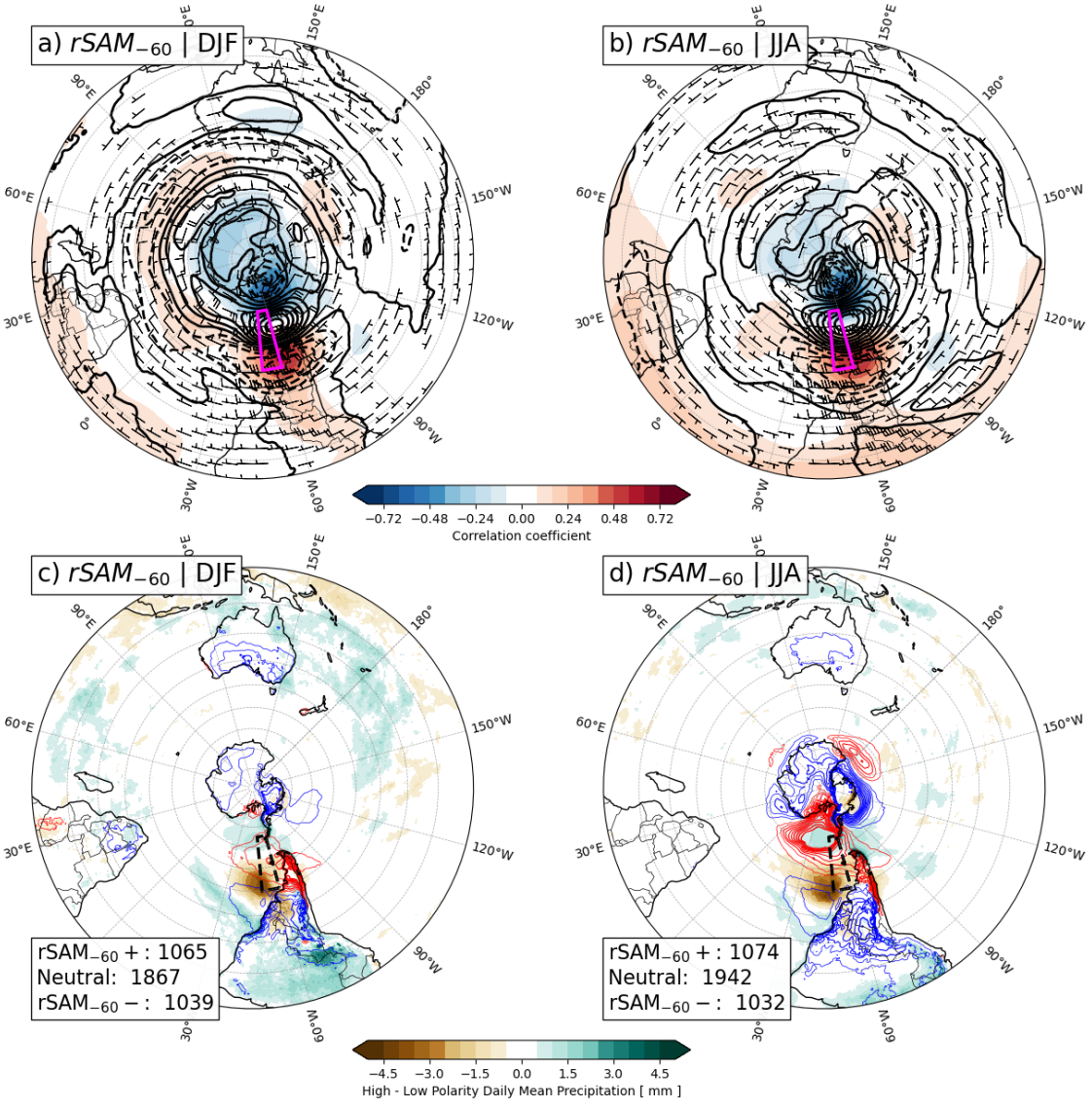

Figure A3. Circulation and weather associated with rSAM in the 60°W longitude band representing the southwestern Australian region. Panels a and b: As in Figure 2c,d. Panels c and d: As in Figure 3c,d.

Author contributions. MAB was responsible for all writing, analysis and figure generation in this study. All authors were involved in the conceptualisation of the work, while editing and revision of the method was done by JSR, TJP, CT and NE-J. The methods were created and refined by all authors.

https://doi.org/10.5194/egusphere-2026-3141
Preprint. Discussion started: 17 June 2026

Competing interests. No competing interests are present.

Acknowledgements. This project was undertaken with the assistance of resources and services from Monash University and Australia's National Computational Infrastructure (NCI). MAB is funded by the Australian Research Council (ARC) Centre of Excellence for the Weather of the 21st Century (CE230100012). JSR, TJP, CT and DM are supported by the Victorian Water and Climate Initiative of the Victorian Department of Energy, Environment and Climate Action.

https://doi.org/10.5194/egusphere-2026-3141
Preprint. Discussion started: 17 June 2026

References

Barnes, E. A. and Hartmann, D. L.: Dynamical Feedbacks of the Southern Annular Mode in Winter and Summer, Journal of the Atmospheric Sciences, 67, 2320–2330, https://doi.org/10.1175/2010JAS3385.1, 2010.

Barnes, E. A. and Hartmann, D. L.: Detection of Rossby Wave Breaking and Its Response to Shifts of the Midlatitude Jet with Climate Change, Journal of Geophysical Research Atmospheres, 117, 1–17, https://doi.org/10.1029/2012jd017469, 2012.

Barnes, M. A., Ndarana, T., and Landman, W. A.: Cut-off Lows in the Southern Hemisphere and Their Extension to the Surface, Climate Dynamics, 56, 3709–3732, https://doi.org/10.1007/s00382-021-05662-7, 2021.

Barnes, M. A., Ndarana, T., Sprenger, M., and Landman, W. A.: Stratospheric Intrusion Depth and Its Effect on Surface Cyclogenetic Forcing: An Idealized Potential Vorticity (PV) Inversion Experiment, Weather and Climate Dynamics, 3, 1291–1309, https://doi.org/10.5194/wcd-3-1291-2022, 2022.

Barnes, M. A., Reeder, M. J., and Ndarana, T.: Rossby Wave Breaking Morphologies on the Southern Hemisphere Dynamical Tropopause, Journal of Climate, https://doi.org/10.1175/JCLI-D-24-0461.1, 2025.

Benedict, J. J., Lee, S., and Feldstein, S. B.: Synoptic View of the North Atlantic Oscillation, Journal of the Atmospheric Sciences, 61, 121–144, https://doi.org/10.1175/1520-0469(2004)061<0121:SVOTNA>2.0.CO;2, 2004.

Berrisford, P., Hoskins, B. J., and Tyrlis, E.: Blocking and Rossby Wave Breaking on the Dynamical Tropopause in the Southern Hemisphere, Journal of the Atmospheric Sciences, 64, 2881–2898, https://doi.org/10.1175/jas3984.1, 2007.

Bowley, K. A., Gyakum, J. R., and Atallah, E. H.: A New Perspective toward Cataloging Northern Hemisphere Rossby Wave Breaking on the Dynamic Tropopause, Monthly Weather Review, 147, 409–431, https://doi.org/10.1175/mwr-d-18-0131.1, 2019.

Brahmananda Rao, V., Do Carmo, A. M. C., and Franchito, S. H.: Interannual Variations of Storm Tracks in the Southern Hemisphere and Their Connections with the Antarctic Oscillation, International Journal of Climatology, 23, 1537–1545, https://doi.org/10.1002/joc.948, 2003.

Campitelli, E., Díaz, L. B., and Vera, C.: Assessment of Zonally Symmetric and Asymmetric Components of the Southern Annular Mode Using a Novel Approach, Climate Dynamics, 58, 161–178, https://doi.org/10.1007/s00382-021-05896-5, 2022.

Copernicus Climate Change Service: ERA5 hourly data on pressure levels from 1940 to present [Dataset], https://doi.org/10.24381/CDS.BD0915C6, 2018a.

Copernicus Climate Change Service: ERA5 hourly data on single levels from 1940 to present [Dataset], https://doi.org/10.24381/CDS.ADBB2D47, 2018b.

Ding, Q., Steig, E. J., Battisti, D. S., and Wallace, J. M.: Influence of the Tropics on the Southern Annular Mode, Journal of Climate, 25, 6330–6348, https://doi.org/10.1175/jcli-d-11-00523.1, 2012.

Fogt, R. L., Jones, J. M., and Renwick, J.: Seasonal Zonal Asymmetries in the Southern Annular Mode and Their Impact on Regional Temperature Anomalies, Journal of Climate, 25, 6253–6270, https://doi.org/10.1175/JCLI-D-11-00474.1, 2012.

Franzke, C., Lee, S., and Feldstein, S. B.: Is the North Atlantic Oscillation a Breaking Wave?, Journal of the Atmospheric Sciences, 61, 145–160, https://doi.org/10.1175/1520-0469(2004)061<0145:ITNAOA>2.0.CO;2, 2004.

Gerber, E. P. and Vallis, G. K.: A Stochastic Model for the Spatial Structure of Annular Patterns of Variability and the North Atlantic Oscillation, Journal of Climate, 18, 2102–2118, https://doi.org/10.1175/JCLI3337.1, 2005.

Gillett, Z. E., Hendon, H. H., Arblaster, J. M., Lin, H., and Fuchs, D.: On the Dynamics of Indian Ocean Teleconnections into the Southern Hemisphere during Austral Winter, Journal of the Atmospheric Sciences, https://doi.org/10.1175/jas-d-21-0206.1, 2022.

https://doi.org/10.5194/egusphere-2026-3141
Preprint. Discussion started: 17 June 2026

Gong, D. and Wang, S.: Definition of Antarctic Oscillation Index, Geophysical Research Letters, 26, 459–462, https://doi.org/10.1029/1999GL900003, 1999.

Hendon, H. H., Thompson, D. W. J., and Wheeler, M. C.: Australian Rainfall and Surface Temperature Variations Associated with the Southern Hemisphere Annular Mode, Journal of Climate, 20, 2452–2467, https://doi.org/10.1175/JCLI4134.1, 2007.

Hersbach, H., Bell, B., Berrisford, P., Hirahara, S., Horányi, A., Muñoz-Sabater, J., Nicolas, J., Peubey, C., Radu, R., Schepers, D., Simmons, A., Soci, C., Abdalla, S., Abellan, X., Balsamo, G., Bechtold, P., Biavati, G., Bidlot, J., Bonavita, M., Chiara, G. D., Dahlgren, P., Dee, D., Diamantakis, M., Dragani, R., Flemming, J., Forbes, R., Fuentes, M., Geer, A., Haimberger, L., Healy, S., Hogan, R. J., Hólm, E., Janisková, M., Keeley, S., Laloyaux, P., Lopez, P., Lupu, C., Radnoti, G., rosnayde Rosnay, P., Rozum, I., Vamborg, F., Villaume, S., and Thépaut, J. N.: The ERA5 Global Reanalysis, Quarterly Journal of the Royal Meteorological Society, 146, 1999–2049, https://doi.org/10.1002/qj.3803, 2020.

Hoskins, B. J., McIntyre, M. E., and Robertson, A. W.: On the Use and Significance of Isentropic Potential Vorticity Maps, Quarterly Journal of the Royal Meteorological Society, 111, 877–946, https://doi.org/10.1002/qj.49711147002, 1985.

Kaderli, S.: Skaderli/WaveBreaking: WaveBreaking v0.3.8, Zenodo, https://doi.org/10.5281/ZENODO.14214463, 2024.

Koch, P., Wernli, H., and Davies, H. C.: An Event-based Jet-stream Climatology and Typology, International Journal of Climatology, 26, 283–301, https://doi.org/10.1002/joc.1255, 2006.

Lim, E.-P., Hendon, H. H., Arblaster, J. M., Delage, F., Nguyen, H., Min, S.-K., and Wheeler, M. C.: The Impact of the Southern Annular Mode on Future Changes in Southern Hemisphere Rainfall, Geophysical Research Letters, 43, 7160–7167, https://doi.org/10.1002/2016GL069453, 2016.

Lim, E.-P., Hendon, H. H., Butler, A. H., Thompson, D. W. J., Lawrence, Z. D., Scaife, A. A., Shepherd, T. G., Polichtchouk, I., Nakamura, H., Kobayashi, C., Comer, R., Coy, L., Dowdy, A., Garreaud, R. D., Newman, P. A., and Wang, G.: The 2019 Southern Hemisphere Stratospheric Polar Vortex Weakening and Its Impacts, Bulletin of the American Meteorological Society, 102, E1150–E1171, https://doi.org/10.1175/BAMS-D-20-0112.1, 2021.

Luo, D., Lupo, A. R., and Wan, H.: Dynamics of Eddy-Driven Low-Frequency Dipole Modes. Part I: A Simple Model of North Atlantic Oscillations, Journal of the Atmospheric Sciences, 64, 3–28, https://doi.org/10.1175/JAS3818.1, 2007.

Marshall, G. J.: Trends in the Southern Annular Mode from Observations and Reanalyses, Journal of Climate, 16, 4134–4143, https://doi.org/10.1175/1520-0442(2003)016<4134:TITSAM>2.0.CO;2, 2003.

Marshall, J., Kushnir, Y., Battisti, D., Chang, P., Czaja, A., Dickson, R., Hurrell, J., McCartney, M., Saravanan, R., and Visbeck, M.: North Atlantic Climate Variability: Phenomena, Impacts and Mechanisms, International Journal of Climatology, 21, 1863–1898, https://doi.org/10.1002/joc.693, 2001.

Mcintyre, M. E. and Palmer, T. N.: Breaking Planetary Waves in the Stratosphere, Nature, 305, 593–600, https://doi.org/10.1038/305593a0, 1983.

Meneghini, B., Simmonds, I., and Smith, I. N.: Association between Australian Rainfall and the Southern Annular Mode, International Journal of Climatology, 27, 109–121, https://doi.org/10.1002/joc.1370, 2007.

NCI Australia: ERA5 Replicated Datasets [Dataset], https://dx.doi.org/10.25914/5f48874388857, 2020.

Ndarana, T. and Waugh, D. W.: The Link between Cut-off Lows and Rossby Wave Breaking in the Southern Hemisphere, Quarterly Journal of the Royal Meteorological Society, 136, 869–885, https://doi.org/10.1002/qj.627, 2010.

Ndarana, T. and Waugh, D. W.: A Climatology of Rossby Wave Breaking on the Southern Hemisphere Tropopause, Journal of the Atmospheric Sciences, 68, 798–811, https://doi.org/10.1175/2010jas3460.1, 2011.

https://doi.org/10.5194/egusphere-2026-3141
Preprint. Discussion started: 17 June 2026

Nicholls, N.: Local and Remote Causes of the Southern Australian Autumn-Winter Rainfall Decline, 1958–2007, Climate Dynamics, 34, 835–845, https://doi.org/10.1007/s00382-009-0527-6, 2010.

Pelly, J. L. and Hoskins, B. J.: A New Perspective on Blocking, Journal of the Atmospheric Sciences, 60, 743–755, https://doi.org/10.1175/1520-0469(2003)060<0743:ANPOB>2.0.CO;2, 2003.

Pezza, A. B., Durrant, T., Simmonds, I., and Smith, I.: Southern Hemisphere Synoptic Behavior in Extreme Phases of SAM, ENSO, Sea Ice Extent, and Southern Australia Rainfall, Journal of Climate, 21, 5566–5584, https://doi.org/10.1175/2008JCLI2128.1, 2008.

Purich, A., Cai, W., England, M. H., and Cowan, T.: Evidence for Link between Modelled Trends in Antarctic Sea Ice and Underestimated Westerly Wind Changes, Nature Communications, 7, 10 409, https://doi.org/10.1038/ncomms10409, 2016.

Purich, A., Arblaster, J. M., Boschat, G., Gillett, Z. E., Hobbs, W., Jucker, M., Lim, E.-P., Udy, D., Abram, N., Campitelli, E., Doddridge, E., England, M. H., King, A., Menviel, L., Meyer, A., Ortiz Guzmán, V., Roy, R., Rudeva, I., Spence, P., Strutton, P. G., and Ziehn, T.: Southern Annular Mode Dynamics, Projections and Impacts in a Changing Climate, Nature Reviews Earth & Environment, https://doi.org/10.1038/s43017-025-00746-y, 2025.

Reeder, M. J., Spengler, T., and Musgrave, R.: Rossby Waves, Extreme Fronts, and Wildfires in Southeastern Australia, Geophysical Research Letters, 42, 2015–2023, https://doi.org/10.1002/2015gl063125, 2015.

Reid, K. J., Arblaster, J. M., Alexander, L. V., and Siems, S. T.: Spurious Trends in High Latitude Southern Hemisphere Precipitation Observations, Geophysical Research Letters, 51, e2023GL106 994, https://doi.org/10.1029/2023GL106994, 2024.

Risbey, J. S., Monselesan, D. P., Black, A. S., Moore, T. S., Richardson, D., Squire, D. T., and Tozer, C. R.: The Identification of Long-Lived Southern Hemisphere Flow Events Using Archetypes and Principal Components, Monthly Weather Review, https://doi.org/10.1175/MWR-D-20-0314.1, 2021.

Scherrer, S. C., Croci-Maspoli, M., Schwierz, C., and Appenzeller, C.: Two-Dimensional Indices of Atmospheric Blocking and Their Statistical Relationship with Winter Climate Patterns in the Euro-Atlantic Region, International Journal of Climatology, 26, 233–249, https://doi.org/10.1002/joc.1250, 2006.

Sen Gupta, A. and England, M. H.: Coupled Ocean–Atmosphere–Ice Response to Variations in the Southern Annular Mode, Journal of Climate, 19, 4457–4486, https://doi.org/10.1175/JCLI3843.1, 2006.

Shabbar, A., Huang, J., and Higuchi, K.: The Relationship between the Wintertime North Atlantic Oscillation and Blocking Episodes in the North Atlantic, International Journal of Climatology, 21, 355–369, https://doi.org/10.1002/joc.612, 2001.

Simpson, I. R. and Polvani, L. M.: Revisiting the Relationship between Jet Position, Forced Response, and Annular Mode Variability in the Southern Midlatitudes, Geophysical Research Letters, 43, 2896–2903, https://doi.org/10.1002/2016GL067989, 2016.

Spensberger, C., Reeder, M. J., Spengler, T., and Patterson, M.: The Connection between the Southern Annular Mode and a Feature-Based Perspective on Southern Hemisphere Midlatitude Winter Variability, Journal of Climate, 33, 115–129, https://doi.org/10.1175/jcli-d-19-0224.1, 2020.

Sprenger, M., Fragkoulidis, G., Binder, H., Croci-Maspoli, M., Graf, P., Grams, C. M., Knippertz, P., Madonna, E., Schemm, S., Škerlak, B., and Wernli, H.: Global Climatologies of Eulerian and Lagrangian Flow Features Based on ERA-Interim, Bulletin of the American Meteorological Society, 98, 1739–1748, https://doi.org/10.1175/BAMS-D-15-00299.1, 2017.

Thompson, D. W. J. and Wallace, J. M.: Annular Modes in the Extratropical Circulation. Part I: Month-to-Month Variability, Journal of Climate, 13, 1000–1016, https://doi.org/10.1175/1520-0442(2000)013<1000:AMITEC>2.0.CO;2, 2000.

Trewin, B.: Climate Summary for the Southern Hemisphere, 2019–20: A Strong Positive Indian Ocean Dipole, Journal of Southern Hemisphere Earth Systems Science, 74, https://doi.org/10.1071/ES24015, 2024.

https://doi.org/10.5194/egusphere-2026-3141
Preprint. Discussion started: 17 June 2026

Wang, Y. H. and Magnusdottir, G.: Tropospheric Rossby Wave Breaking and the SAM, Journal of Climate, 24, 2134–2146, https://doi.org/10.1175/2010jcli4009.1, 2011.

Wernli, H. and Schwierz, C.: Surface Cyclones in the ERA-40 Dataset (1958–2001). Part I: Novel Identification Method and Global Climatology, Journal of the Atmospheric Sciences, 63, 2486–2507, https://doi.org/10.1175/JAS3766.1, 2006.

Woollings, T., Hoskins, B., Blackburn, M., and Berrisford, P.: A New Rossby Wave–Breaking Interpretation of the North Atlantic Oscillation, Journal of the Atmospheric Sciences, 65, 609–626, https://doi.org/10.1175/2007JAS2347.1, 2008.